PLOS ONE

RESEARCH ARTICLE

Ocular and uteroplacental pathology in a macaque pregnancy with congenital Zika virus infection

Emma L. Mohr[1☯]*, Lindsey N. Block[2☯], Christina M. Newman[2☯], Laurel M. Stewart[2], Michelle Koenig[2], Matthew Semler[2], Meghan E. Breitbach[2], Leandro B. C. Teixeira[3], Xiankun Zeng[4], Andrea M. Weiler[5], Gabrielle L. Barry[5], Troy H. Thoong[5], Gregory J. Wiepz[5], Dawn M. Dudley[2], Heather A. Simmons[5], Andres Mejia[5], Terry K. Morgan[6], M. Shahriar Salamat[2], Sarah Kohn[7], Kathleen M. Antony[8], Matthew T. Aliota[3], Mariel S. Mohns[2], Jennifer M. Hayes[5], Nancy Schultz-Darken[5], Michele L. Schotzko[5], Eric Peterson[5], Saverio Capuano, III[5], Jorge E. Osorio[3], Shelby L. O'Connor[2], Thomas C. Friedrich[3,5], David H. O'Connor[2,5], Thaddeus G. Golos[5,8,9]*

1 Department of Pediatrics, University of Wisconsin-Madison, Madison, Wisconsin, United States of America, **2** Department of Pathology and Laboratory Medicine, University of Wisconsin-Madison, Madison, Wisconsin, United States of America, **3** Department of Pathobiological Sciences, University of Wisconsin-Madison, Madison, Wisconsin, United States of America, **4** United States Army Medical Research Institute of Infectious Diseases, Fort Detrick, Frederick, Maryland, United States of America, **5** Wisconsin National Primate Research Center, University of Wisconsin-Madison, Madison, Wisconsin, United States of America, **6** Departments of Pathology and Obstetrics & Gynecology, Oregon Health & Science University, Portland, Oregon, United States of America, **7** Department of Radiology, University of Wisconsin-Madison, Madison, Wisconsin, United States of America, **8** Department of Obstetrics and Gynecology, University of Wisconsin-Madison, Madison, Wisconsin, United States of America, **9** Department of Comparative Biosciences, University of Wisconsin-Madison, Madison, Wisconsin, United States of America

☯ These authors contributed equally to this work.
* emohr@uwhealth.org (ELM); golos@primate.wisc.edu (TGG)

OPEN ACCESS

Citation: Mohr EL, Block LN, Newman CM, Stewart LM, Koenig M, Semler M, et al. (2018) Ocular and uteroplacental pathology in a macaque pregnancy with congenital Zika virus infection. PLoS ONE 13 (1): e0190617. https://doi.org/10.1371/journal.pone.0190617

Editor: Michael R Holbrook, NIAID Integrated Research Facility, UNITED STATES

Received: September 29, 2017

Accepted: December 18, 2017

Published: January 30, 2018

Data Availability Statement: All relevant data are within the paper and its Supporting Information files.

Funding: This study was supported by the National Institutes of Health (R21 HD091163-01, R01 AI116382-01A1S1, P51 OD011106, T32 AI55397) and the Pediatric Infectious Diseases Society. The funders had no role in study design, data collection and analysis, decision to publish, or preparation of the manuscript. Opinions, interpretations, conclusions, and recommendations are those of

Abstract

Congenital Zika virus (ZIKV) infection impacts fetal development and pregnancy outcomes. We infected a pregnant rhesus macaque with a Puerto Rican ZIKV isolate in the first trimester. The pregnancy was complicated by preterm premature rupture of membranes (PPROM), intraamniotic bacterial infection and fetal demise 49 days post infection (gestational day 95). Significant pathology at the maternal-fetal interface included acute chorioamnionitis, placental infarcts, and leukocytoclastic vasculitis of the myometrial radial arteries. ZIKV RNA was disseminated throughout fetal tissues and maternal immune system tissues at necropsy, as assessed by quantitative RT-PCR for viral RNA. Replicating ZIKV was identified in fetal tissues, maternal uterus, and maternal spleen by fluorescent in situ hybridization for viral replication intermediates. Fetal ocular pathology included a choroidal coloboma, suspected anterior segment dysgenesis, and a dysplastic retina. This is the first report of ocular pathology and prolonged viral replication in both maternal and fetal tissues following congenital ZIKV infection in a rhesus macaque. PPROM followed by fetal demise and severe pathology of the visual system have not been described in macaque congenital ZIKV infection previously. While this case of ZIKV infection during pregnancy was complicated by bacterial infection with PPROM, the role of ZIKV on this outcome cannot be precisely defined, and further nonhuman primate studies will determine if increased risk for

the author (X. Zeng) and are not necessarily endorsed by the U.S. Army.

Competing interests: The authors have declared that no competing interests exist.

PPROM or other adverse pregnancy outcomes are associated with congenital ZIKV infection.

Introduction

First isolated from a febrile rhesus macaque in Uganda in 1947, Zika virus (ZIKV) generally did not result in recognized widespread clinical disease in subsequent outbreaks across Asia and the South Pacific, until late 2015, when clinicians in Northeast Brazil reported a surge in babies born with severe birth defects [1]. By early 2016, the US Centers for Disease Control and Prevention (CDC) asserted that there was a causal relationship between prenatal ZIKV infection and serious brain anomalies including microcephaly [2]. The constellation of fetal and neonatal abnormalities and birth defects associated with ZIKV infection *in utero* is designated congenital Zika syndrome (CZS) [3–9]. Characteristics of CZS include ocular anomalies, brain anomalies, stillbirth, cranial dysmorphologies, musculoskeletal contractures and neurologic sequelae [10]. Infection during the first trimester increases the risk for birth defects [5] because critical cell proliferation and differentiation occurs during this trimester [11]. One striking characteristic of CZS is a high frequency of ocular malformations, observed in as many as 55% of infants with evidence of congenital ZIKV infection and microcephaly [12, 13]. Multiple case reports and case series have identified infants with ocular anomalies, which include macular pigment mottling, optic nerve hypoplasia, chorioretinal and iris coloboma, lens subluxation, retinal vascular abnormalities, cataracts and maculopathy [5, 14–21]. Specific retinal defects include retinal thinning, discontinuity of the retinal pigment epithelium, and colobomatous-like excavation in the neurosensory retina, retinal pigment epithelium and choroid in multiple infants [17]. Because the retina develops as an outpocketing from the neural tube [22], the presence of retinal lesions is consistent with CNS damage in CZS.

Other recognized outcomes of congenital ZIKV infection are miscarriage, stillbirth and PPROM [23–26]. The etiology of PPROM is multifactorial [27]. Prenatal ZIKV infection in the first trimester of gestation results in up to 25% of pregnancies with miscarriage, fetal loss or stillbirth, with lower frequencies in the second and third trimesters in a study including 125 pregnancies [28]. The CDC reports 15 fetal demise cases with birth defects out of 4,695 live births in women with confirmed ZIKV infection [29]. However, this number likely does not capture the total number of fetal demises following congenital ZIKV infection because it does not include fetuses without overt birth defects even though there may be vertical transmission, or early pregnancy losses from women who were not aware of infection, or never sought a diagnosis. The pathophysiology of preterm birth or fetal loss before viability following congenital ZIKV infection has not been defined. In murine models, pregnancy following a systemic viral infection can result in an ascending bacterial uterine infection, inflammation, and preterm birth [30]. It has also been reported that viral persistence of ZIKV in the lower female genital tract in the rhesus monkey is prolonged in animals treated with Depo-Provera, a synthetic progestogen [31]. The specific etiology of adverse pregnancy outcomes in congenital ZIKV infection, however, is yet to be defined and requires further study.

A novel feature of ZIKV infection is the persistence of both ZIKV RNA [32–37] and replication competent virus in some body fluids [33, 38] for weeks after infection. ZIKV RNA has been identified in semen between 3–188 days after infection [39, 40] with a median of 34 days [32] whereas DENV RNA persistence in semen has not been described [41]. DENV RNA may persist in urine longer than ZIKV RNA, with ZIKV RNA identified in urine up to 29 days after

infection [42] with a median of 8 days [32] and DENV RNA isolated from urine up to typically 3–4 weeks after infection [43]. Both ZIKV and DENV RNA have been identified in saliva, with ZIKV RNA identified in saliva up to 29 days after infection [42] and DENV RNA isolated from saliva up to 18 days after symptom onset [44]. Duration of viremia in nonpregnant hosts is similar, with ZIKV RNA identified in serum a median of 14 days after infection [32] and DENV RNA identified up to 10 days after symptom onset [41]. ZIKV persists longer in breast milk, with ZIKV RNA and infectious particles have been isolated from breast milk 2 days after infection [45] and DENV RNA only isolated from breast milk around the time of acute infection [46]. One key difference between ZIKV and DENV infection is the duration of plasma viremia during pregnancy. ZIKV viremia during pregnancy can be prolonged >28 days after infection [25, 47–49], whereas prolonged DENV plasma viremia has only been reported in hematopoietic stem cell recipients [41, 50].

Defining the body fluid and tissue persistence of ZIKV is critical to the development of public health recommendations and solid organ and hematopoietic stem cell transplant guidelines.

Non-human primate (NHP) models have begun to define the tissue distribution of ZIKV following infection because defining tissue distribution in humans is not possible. Following ZIKV infection in nonpregnant NHPs, ZIKV has been identified in multiple tissues up to 35 days after infection, including the brain, spinal cord, eye, spleen, lymph nodes, muscles and joints [51, 52] and in cerebrospinal fluid (CSF) up to 42 days after infection [53, 54], suggesting that one of these tissues may support prolonged ZIKV replication. Since prolonged ZIKV viremia is a feature of ZIKV infection during pregnancy, we hypothesized that ZIKV tissue persistence would be longer in pregnant NHPs compared to nonpregnant NHPs. Indeed, following ZIKV infection in pregnant NHPs, ZIKV RNA detection in plasma is prolonged [51] and can be detected up to 70 days after infection [55], far longer than the plasma viremia duration reported for nonpregnant NHPs [52, 56].

NHP models of both congenital infection and tissue distribution following ZIKV infection provide insight into the pathophysiology of ZIKV infection not possible through epidemiological and clinical human studies. As with humans, the rhesus macaque placenta has a hemochorial placentation with extensive endovascular invasion of the maternal endometrial spiral arterioles and arteries and innate immune cellular populations homologous with that found in the human decidua [57–59]. There are multiple similarities between human and NHP ZIKV infection natural history, including the duration of viremia and viruria [51, 52, 54, 56], robust neutralizing antibody responses [51, 54, 56, 60], vertical transmission [55], and fetal pathology [55, 61]. To define the tissue distribution of ZIKV and fetal pathology following infection with a clinically relevant Puerto Rican isolate of ZIKV, we infected a pregnant rhesus macaque in the first trimester and performed a necropsy of the dam and fetus to comprehensively define maternal and fetal viral tissue distribution following spontaneous fetal death 49 days post-infection. Here, we describe the pregnancy outcome, maternal and fetal viral tissue distribution, and fetal pathology associated with first trimester ZIKV infection in a case of fetal demise.

Materials & methods

Study design

A 3.8 year old, primigravida rhesus macaque (*Macaca mulatta*) of Indian ancestry was infected subcutaneously with $1x10^4$ PFU Zika virus/H.sapiens-tc/PUR/2015/PRVABC59_v3c2 (PRVABC59) during the first trimester, 46 days gestation (term 165±10 days). This macaque was part of the Specific Pathogen Free (SPF) colony at the Wisconsin National Primate

Research Center (WNPRC) and was free of Macacine herpesvirus 1 (Herpes B), Simian Retrovirus Type D (SRV), Simian T-lymphotropic virus Type 1 (STLV), and Simian Immunodeficiency Virus (SIV).

Ethics

All monkeys are cared for by the staff at the WNPRC in accordance with the regulations and guidelines outlined in the Animal Welfare Act and the Guide for the Care and Use of Laboratory Animals and the recommendations of the Weatherall report (https://royalsociety.org/topics-policy/publications/2006/weatherall-report/). Per WNPRC standard operating procedures for animals assigned to protocols involving the experimental inoculation of an infectious pathogen, environmental enhancement included constant visual, auditory, and olfactory contact with conspecifics, the provision of feeding devices which inspire foraging behavior, the provision and rotation of novel manipulanda (e.g., Kong toys, nylabones, etc.), and enclosure furniture (i.e., perches, shelves). Per Animal Welfare Regulations (Title 9, Chapter 1, Subchapter A, Parts 1–4, Section 3.80 Primary enclosures) the animal was housed in a nonhuman primate Group 3 enclosure with at least 4.3 square feet of floor space and at least 30 inches of height. This study was approved by the University of Wisconsin-Madison Graduate School Institutional Animal Care and Use Committee (animal protocol number G005401).

Care & use of macaques

The female monkey described in this report was co-housed with a compatible male and observed daily for menses and breeding. Pregnancy was detected by ultrasound examination of the uterus at approximately 20–24 gestation days (gd) following the predicted day of ovulation. The gd was estimated (+/- 2 days) based on the dam's menstrual cycle, observation of copulation, and the greatest length of the fetus at initial ultrasound examination which was compared to normative growth data in this species [62]. For physical examinations, virus inoculations, some ultrasound examinations, blood and swab collections, the dam was anesthetized with an intramuscular dose of ketamine (10 mg/kg). Blood samples from the femoral or saphenous vein were obtained using a vacutainer system or needle and syringe. The pregnant macaque was monitored daily prior to and after inoculation for any clinical signs of infection (e.g., diarrhea, inappetence, inactivity and atypical behaviors). This macaque developed chronic diarrhea prior to conception which was controlled by daily treatment with oral tylosin while pregnant. This is a standard treatment in the WNPRC colony and has not been associated with any adverse pregnancy outcomes in nonhuman primates.

Inoculation and monitoring

ZIKV strain PRVABC59 (GenBank: KU501215), originally isolated from a traveler to Puerto Rico and passaged three times on Vero cells (American Type Culture Collection (ATCC): CCL-81), was obtained from Brandy Russell (CDC, Ft. Collins, CO). Virus stocks were prepared by inoculation onto a confluent monolayer of C6/36 cells (*Aedes albopictus* larval cells; ATCC: CCL-1660) with two rounds of amplification. The inoculating stock was prepared and validated as previously described [55, 56]. The animal was anesthetized as described above, and 1 mL of inoculum at 1 x 10^4 PFU dilution in PBS was administered subcutaneously over the cranial dorsum at 46 days of gestation. Post-inoculation, the animal was closely monitored by veterinary and animal care staff for adverse reactions or any signs of disease.

Pregnancy monitoring and fetal measurements

Weekly ultrasounds were conducted to observe the health of the fetus and to obtain measurements including fetal femur length (FL), biparietal diameter (BPD), head circumference (HC), and heart rate, with methods as previously described [55]. Growth curves were developed for FL, BPD, and HC [63]. Mean measurements and standard deviations at specified days of gestation in rhesus macaques were retrieved from Tarantal et al. [62] and the data were plotted against normative data for fetal rhesus macaques [63]. The actual growth measurements were obtained from weekly ultrasound data and used to retrieve the predicted growth measurement by plotting the obtained experimental growth measurement against the growth curves. Data were then graphed as actual gestation age versus predicted gestation age to depict rate of growth compared to uninfected, control rhesus macaques (method described previously in [55]). Doppler ultrasounds to measure fetal heart rate were performed as requested by veterinary staff.

Amniocentesis

For amniocentesis, the animal was shaved and the skin was prepped with Betadyne® solution. Sterile syringes, needles and gloves were used during the amniocentesis procedure. Under real-time ultrasound guidance, a 22 gauge, 3.5 inch Quincke spinal needle was inserted into the amniotic sac as described previously [55]. The first 1.5–2 mL of fluid was discarded due to potential maternal contamination, and an additional 3–4 mL of amniotic fluid was collected in a new sterile syringe for viral qRT-PCR analysis as described elsewhere [56]. These samples were obtained at the gestational ages specified in Fig 1. All fluids were free of any blood contamination.

vRNA isolation from body fluids and tissues

RNA was isolated from maternal plasma, urine, saliva and amniotic fluid using the Viral Total Nucleic Acid Purification Kit (Promega, Madison, WI, USA) and from maternal and fetal tissues using the Maxwell 16 LEV simplyRNA Tissue Kit (Promega, Madison, WI) on a Maxwell 16 MDx instrument as previously reported [56]. Fetal and maternal tissues were processed with RNAlater® (Invitrogen, Carlsbad, CA) according to manufacturer protocols. 20–40 mg of each tissue was homogenized using homogenization buffer from the Maxwell 16 LEV simplyRNA Tissue Kit and two 5 mm stainless steel beads (Qiagen, Hilden, Germany) in a 2 mL

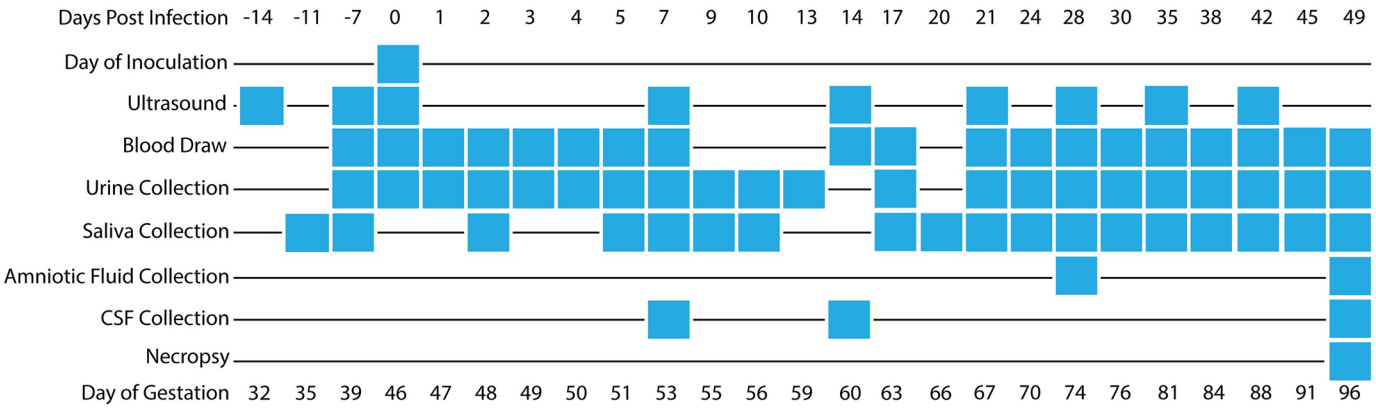

Fig 1. Timeline depicting body fluid sampling and procedures throughout pregnancy. Blood, urine, saliva, amniotic fluid, and CSF were collected as indicated in the schedule above, and ultrasounds were performed weekly. The axes are not drawn to scale.

https://doi.org/10.1371/journal.pone.0190617.g001

snap-cap tube, shaking twice for 3 minutes at 20 Hz each side in a TissueLyser (Qiagen, Hilden, Germany). The isolation was continued according to the Maxwell 16 LEV simplyRNA Tissue Kit protocol, and samples were eluted into 50 μL RNase free water.

Viral quantification by plaque assay

Titrations for replication competent virus quantification of amniotic fluid was completed by plaque assay on Vero cell cultures as described previously [56]. Vero cells were obtained from American Type Culture Collection (CCL-81), were not further authenticated and were not specifically tested for mycoplasma. Duplicate wells were infected with 0.1ml of aliquots from serial 10-fold dilutions in growth media and virus was adsorbed for 1 h. Following incubation, the inoculum was removed, and monolayers were overlaid with 3 ml containing a 1:1 mixture of 1.2% oxoid agar and 2 DMEM (Gibco, Carlsbad, CA, USA) with 10% (vol/vol) FBS and 2% (vol/vol) penicillin/streptomycin. Cells were incubated at 37˚C in 5% CO_2 for 4 days for plaque development. Cell monolayers then were stained with 3 ml of overlay containing a 1:1 mixture of 1.2% oxoid agar and DMEM with 2% (vol/vol) FBS, 2% (vol/vol) penicillin/streptomycin and 0.33% neutral red (Gibco). Cells were incubated overnight at 37˚C and plaques were counted.

Plaque reduction neutralization test (PRNT)

Macaque serum samples were screened for ZIKV neutralizing antibodies utilizing a plaque reduction neutralization test (PRNT). End point titrations of reactive sera, utilizing a 90% cut-off (PRNT90), were performed as described [64] against ZIKV strain PRVABC59. Briefly, ZIKV was mixed with serial 2-fold dilutions of serum for 1 hour at 37˚C prior to being added to Vero cells and neutralization curves were generated using GraphPad Prism software (La Jolla, CA). The resulting data were analyzed by nonlinear regression to estimate the dilution of serum required to inhibit both 90% and 50% of infection.

Maternal and fetal necropsy

At 49 days post infection (dpi) (gd 95), no fetal heartbeat was detected. The dam was sedated, euthanized, and sterile instruments were used for the dissection and collection of all maternal, fetal, and maternal-fetal interface tissues during the gross post-mortem examination. Amniotic fluid was aspirated with a syringe and needle inserted through the uterine wall into the lumen. Each tissue was collected with a unique set of sterile instruments and placed in a separate sterile petri dish before transfer to appropriate containers for viral RNA analysis and histology, to prevent cross-contamination between tissues. Tissue distribution for subsequent analysis was as previously described [55]. Slices of the cerebrum (~5 mm in thickness) were prepared in the coronal plane with section 1 located most anteriorly and section 4 located most posteriorly, and the cerebellum was sectioned in the sagittal plane with section 1 located most laterally; alternate sections were taken for qRT-PCR to analyze vRNA and for histology.

Histology

For general pathology, tissues were fixed in 4% PFA, routinely processed and embedded in paraffin. Paraffin sections (5 μm) were stained with hematoxylin and eosin (H&E) or Gram stain using standard methods. Two veterinary pathologists were blinded to vRNA findings when tissue sections were evaluated microscopically. Lesions in each tissue were described and assigned morphologic diagnoses as described previously [55]. Photomicrographs were obtained using brightfield microscopes Olympus BX43 and Olympus BX46 (Olympus Inc.,

Center Valley, PA) with attached Olympus DP72 digital camera (Olympus Inc.) and Spot Flex 152 64 Mp camera (Spot Imaging, Sterling Heights, MI), and captured using commercially available image-analysis software (cellSens DimensionR, Olympus Inc. and Spot software 5.3). Uteroplacental pathology was specifically performed by an experienced placental pathologist (T.K.M.).

In situ hybridization

In situ hybridization (ISH) was conducted with tissues fixed in 4% PFA, and alcohol processed and paraffin embedded. ISH probes against Zika genome were purchased commercially (Advanced Cell Diagnostics, Cat No. 468361, Newark, California, USA). ISH was performed using the RNAscope® Red 2.5 Kit (Advanced Cell Diagnostics, Cat No. 322350) according to the manufacturer's instructions. Briefly, after deparaffinization with xylene, a series of ethanol washes, and peroxidase blocking, sections were heated in boiling antigen retrieval buffer for 15 minutes and then digested by proteinase K (2.5 μg/ml, to completely cover the section) for 16 minutes at 40˚C. Sections were exposed to ISH target probe and incubated at 40˚C in a hybridization oven for 2 h. After rinsing, ISH signal was amplified using company-provided Pre-amplifier and Amplifier conjugated to horseradish peroxidase (HRP), and incubated with a red substrate-chromogen solution for 10 min at room temperature.

Multiplex fluorescent in situ hybridization

Multiplex fluorescent in situ hybridization (mFISH) was conducted with tissues fixed in 4% PFA. mFISH was performed using the RNAscope® Fluorescent Multiplex Kit (Catalog # 320850, Advanced Cell Diagnostics) according to the manufacturer's instructions with modifications. Probes with C1 channel (Cat# 468361, red) targeting ZIKV positive sense RNA and probes with C3 channel (Cat# 467911, green) targeting ZIKV negative sense RNA were synthesized by Advanced Cell Diagnostics. Paraformaldehyde fixed paraffin embedded rhesus monkey fetus tissue sections underwent deparaffinization with xylene and a series of ethanol washes. These tissue sections were treated with 0.1% Sudan Black B (Sigma-Aldrich, St. Louis, MO, USA) to reduce autofluorescence, heated in antigen retrieval buffer (Citrate buffer with pH 6.0), and digested by proteinase. Sections were exposed to ISH target probes and incubated at 40˚C in a hybridization oven for 2 h. After rinsing, ISH signal was amplified using company-provided Pre-amplifier and Amplifier conjugated to fluorescent dye. Sections were counterstained with 4', 6-diamidino-2-phenylindole (DAPI, Thermo Fisher Scientific, Waltham, MA, USA), mounted, and stored at 4˚C until image analysis. mFISH images were captured on an LSM 880 Confocal Microscope with Airyscan (Zeiss, Oberkochen, Germany) and processed using open-source ImageJ software (National Institutes of Health, Bethesda, MD, USA).

Placental alpha microglobulin-1 (PAMG-1) immunochromatographic assay

A PAMG-1 immunochromatographic assay (AmniSure® ROM (Rupture of [fetal] Membranes) test, Qiagen, Boston, MA, FMRT-1-10-US) was performed according to the manufacturer's protocol with urine and amniotic fluid samples that had been stored at -80˚C. A sterile polyester swab, provided by the manufacturer, was inserted into a tube containing the sample fluid for 1 minute. The swab was then added to the solvent microfuge tube and rotated by hand for 1 minute. Finally, the test strip was placed into the solvent and incubated at room temperature for 10 minutes before the test strip was read and photographs were taken. A term amniotic fluid sample was the positive control and non-pregnant urine was the negative control. Open-source ImageJ software was used to measure the relative pixel density of each band

(control and test band) (National Institutes of Health, Bethesda, MD, USA). The pixel density of each band was measured, the background density was subtracted, and the relative pixel density of each test band was calculated by subtracting the control band density from the test band density.

Insulin-like growth factor-binding protein 1 (IGFBP-1) ELISA

An IGFBP-1 ELISA kit (Abcam, Cambridge, MA, ab100539) was used to determine if a marker for amniotic fluid was detectable in maternal urine. The protocol was followed as specified by the manufacturer and all samples were frozen undiluted at -80˚C until use. Duplicates were run for the standards, samples, positive, and negative controls. A term amniotic fluid sample was used as the positive control and male urine and non-pregnant female urine were used as negative controls. All urine samples were diluted 1:5000 and all amniotic fluid samples were diluted 1:20,000. Immediately upon addition of the stop solution the plate was read at 450 nm. A standard curve was calculated from the average of each standard. This standard curve equation was used to calculate the concentration of each sample.

Results

Pregnancy outcome

The dam had no fever, rash, or inappetence detected following inoculation. The dam's history of chronic diarrhea included 9 episodes of diarrhea during the first 45 days of gestation and no diarrhea following ZIKV inoculation at 46 days of gestation. vRNA titers were monitored in body fluids throughout pregnancy as described in Fig 1. Maternal plasma viremia was detected from days 1 through 18 post-infection, peaking at 5 dpi with 2.55 x 10^5 vRNA copies per mL, and was also detected at 24 dpi (Fig 2). At 21 dpi the viral load dropped below 100 vRNA copies per mL, the limit of quantification of the qRT-PCR assay. Saliva samples remained negative throughout pregnancy. CSF samples taken at 7, 14, and 49 dpi were all negative. In addition to vRNA in these fluids, the development of maternal ZIKV-specific antibodies was assessed. Plaque reduction neutralization tests (PRNT) were performed on serum collected at 10, 28, and 49 dpi. All post-infection time points demonstrated the presence of ZIKV-specific neutralizing antibodies with an increasing concentration of neutralizing antibodies throughout the post-infection period (Fig 3).

Amniotic fluid at 28 dpi had a viral load of 1.84 x 10^4 vRNA copies per mL. The amniotic fluid was reported as clear, and a plaque assay performed on the amniotic fluid was negative. ZIKV RNA was first detected in a passively collected urine sample (i.e. in pan at the bottom of the cage) at 42 dpi, with a concentration of 7 x 10^4 vRNA copies per mL, and was present in the urine until euthanasia at 49 dpi. Because identifying urine vRNA so long after infection was unexpected, and its appearance followed the presence of vRNA in the amniotic fluid, we wanted to determine whether the passively collected urine contained amniotic fluid, a potential harbinger of an adverse pregnancy outcome. We performed an AmniSure® test, which detects an amniotic fluid protein, placental alpha microglobulin-1, (PAMG-1), and determined that urine contained detectable PAMG-1 (Fig 4A and 4B). As expected, the 28 dpi amniotic fluid sample was positive for PAMG-1, as was the positive control term amniotic fluid sample from a different animal. The 28 dpi urine, collected just prior to the amniocentesis, was negative for PAMG-1; however, the 45 and 49 dpi urine samples were positive for PAMG-1. The negative control was a non-pregnant urine sample. AmniSure® is not a quantitative test but the result suggested there was amniotic fluid in the urine samples at 45 and 49 dpi. To confirm this finding, we performed an insulin-like growth factor binding protein-1 (IGFBP-1) ELISA on the animal's pan-collected urine and amniotic fluid samples, along with

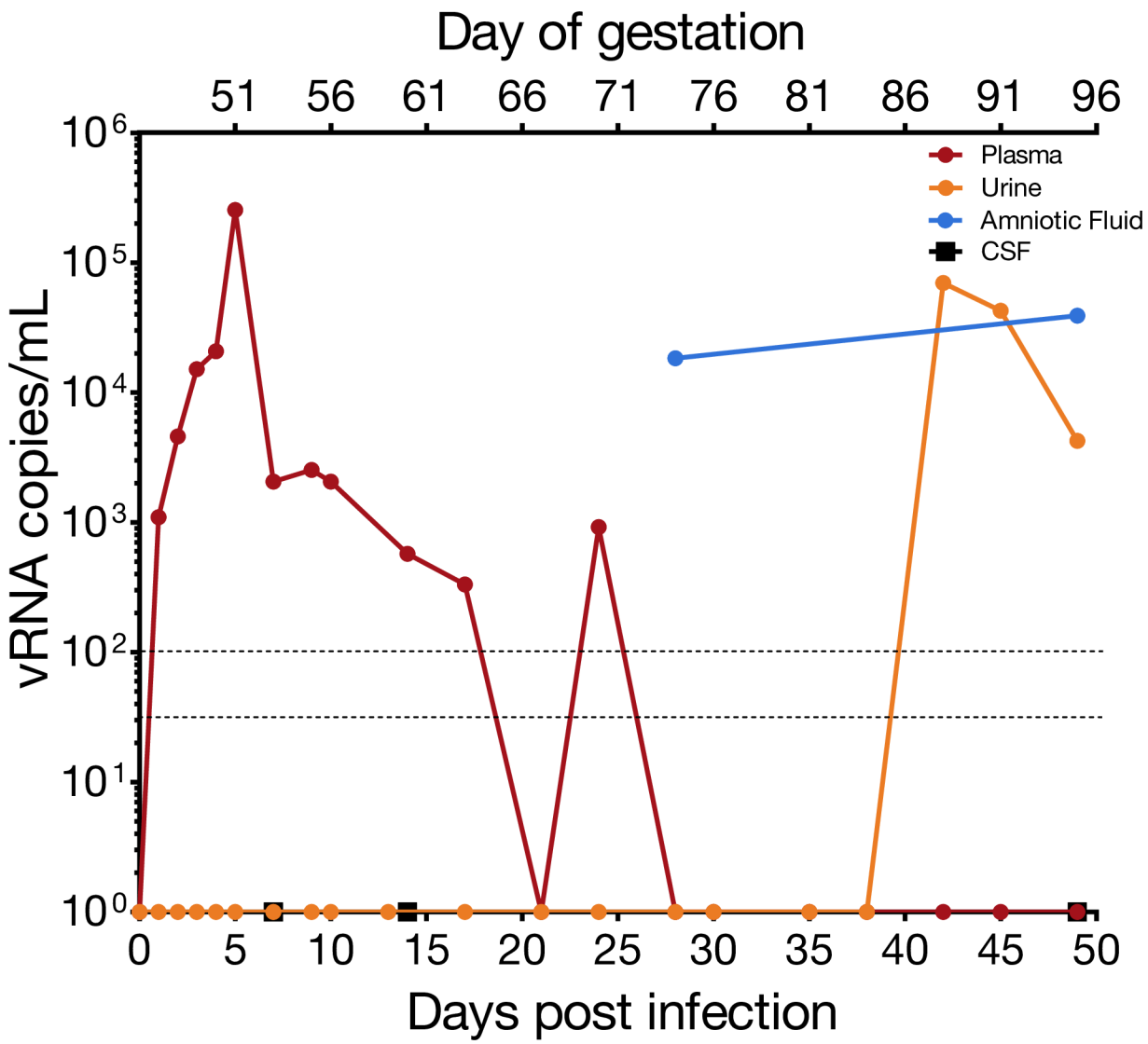

Fig 2. ZIKV RNA levels in maternal body fluids. vRNA was measured by quantitative RT-PCR in plasma, urine, amniotic fluid and CSF. The limit of detection is 33 copies/mL and the assay limit of quantification is 100 copies/mL, which are indicated by dashed lines.

https://doi.org/10.1371/journal.pone.0190617.g002

appropriate controls. IGFBP-1 is a 25 kB protein synthesized and secreted by the fetal liver and maternal decidua, and is present in amniotic fluid from the second trimester of pregnancy until full term [65]. It is not typically found in urine. In the pregnant animal, IGFBP-1 was detected in pan-collected urine at levels similar to that in amniotic fluid alone, confirming the presence of amniotic fluid-specific protein in the pan-collected urine (Fig 4C). The IGFBP-1 levels in urine from this dam were higher than negative control urine samples (urine from a male and a nonpregnant female). The presence of two amniotic fluid markers in the pan-collected urine supports dilution of amniotic fluid in urine and is consistent with premature rupture of membranes.

Ultrasonography

The fetus displayed typical growth in all parameters when compared with normative data (Fig 5) [62] and a comparison of the predicted gestational age (pGA) vs. the clinically estimated

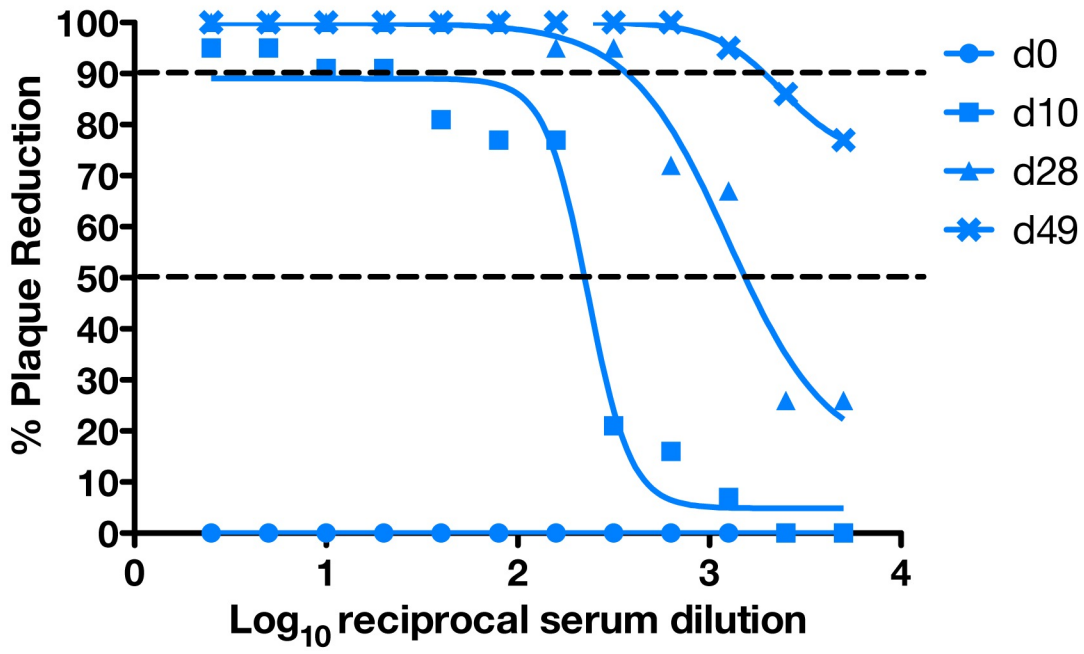

Fig 3. Neutralizing antibody titers following ZIKV infection. PRNT titers were measured pre and post infection. The x-axis represents the reciprocal serum dilution (log_{10}) and the y-axis represents the percent reduction. The dashed lines indicate 90% and 50% reduction.

https://doi.org/10.1371/journal.pone.0190617.g003

(actual) gestational age (aGA) [55, 62] did not reveal any growth trajectory anomalies (Fig 5B growth chart). No significant placental lesions were identified until 35 dpi (gd 81) when ultrasonography identified a possible area of placental abruption and a retroplacental clot along the edge of the placenta over the cervix, which was resolving by 42 dpi (gd 88). No fetal abnormalities were noted at either time point, and the fetus did not demonstrate any persistent tachycardia or bradycardia. Because of these small placental lesions, daily heart rate monitoring was initiated and remained within a normal range until 49 dpi (gd 95) when no fetal heartbeat was detected.

The dam underwent euthanasia and during the necropsy, the cervix was noted to be closed and no debris was noted in the vaginal vault. The amniotic sac contained significant amounts of adherent purulent matter, and purulent fibrinous material covered the decidua and fetus (Fig 6). The fetus showed advanced tissue autolysis, including severe autolysis of the fetal brain. Bacterial culture obtained by swab of the fibrinopurulent amniotic fluid at the time of necropsy demonstrated *Staphylococcus epidermidis*. We also identified clusters of gram positive cocci in the fetal esophageal lumen (S1 Fig). *S. epidermidis* is part of the vaginal flora in rhesus macaques [66]. Bacteria were not detected in any other fetal or maternal histological specimens by gram stain and no additional tissue samples were submitted for bacterial culture.

Fetal and maternal vRNA tissue distribution

ZIKV RNA was widely distributed within fetal tissues, maternal lymphoid structures, and the reproductive tract: 33 fetal, maternal and maternal-fetal interface tissues were positive for vRNA (Table 1 vRNA); of these, 27 were fetal tissues. The presence of vRNA in an adipose tissue/omentum sample is interesting, although we do not know the precise cellular location of vRNA in this sample.

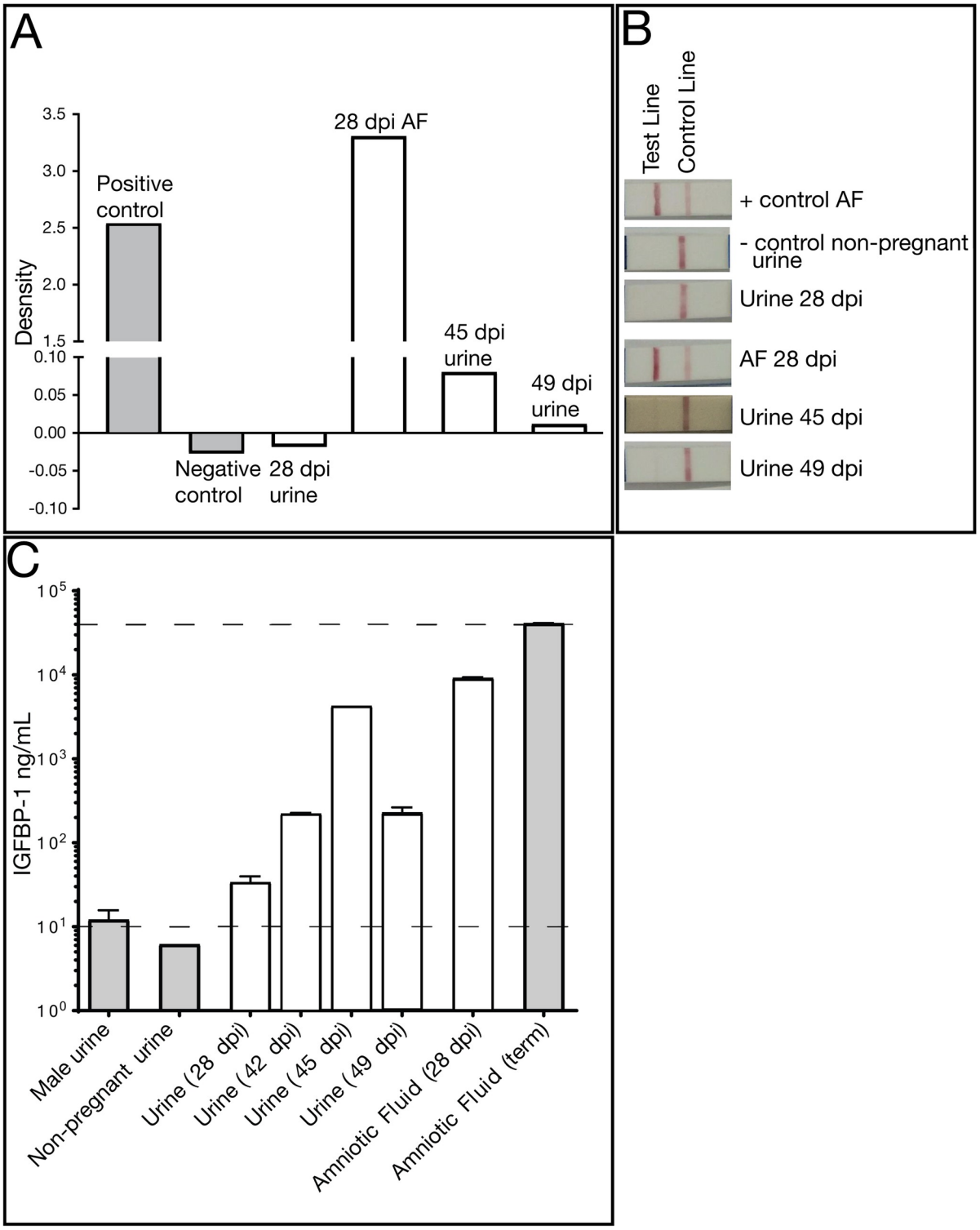

Fig 4. Amniotic fluid (AF) markers confirm rupture of membranes and contamination of pan-collected urine. (A) An AmniSure® test, which measures PAMG-1 protein, was performed on pan urine collection (28 dpi, 45 dpi, 49 dpi) and AF (28 dpi) from the pregnant animal. Nonpregnant control animal urine and pregnant animal AF are included as controls. (B) Relative pixel density of the Amnisure® test strip test band and control band. (C) Amniotic fluid protein IGFBP-1 ELISA. Body fluids from the pregnant animal (pan urine collection 28, 42, 45, 49 dpi and AF 28 dpi), nonpregnant negative control male and female urine samples, amniotic fluid from a control pregnancy were evaluated for the presence of IGFBP-1. Dashed lines indicate the upper and lower limits of quantitative accuracy of the assay. In Panels B and C, white bars denote body fluids from the experimental animal and grey bars denote control fluids from other animals in the colony.

https://doi.org/10.1371/journal.pone.0190617.g004

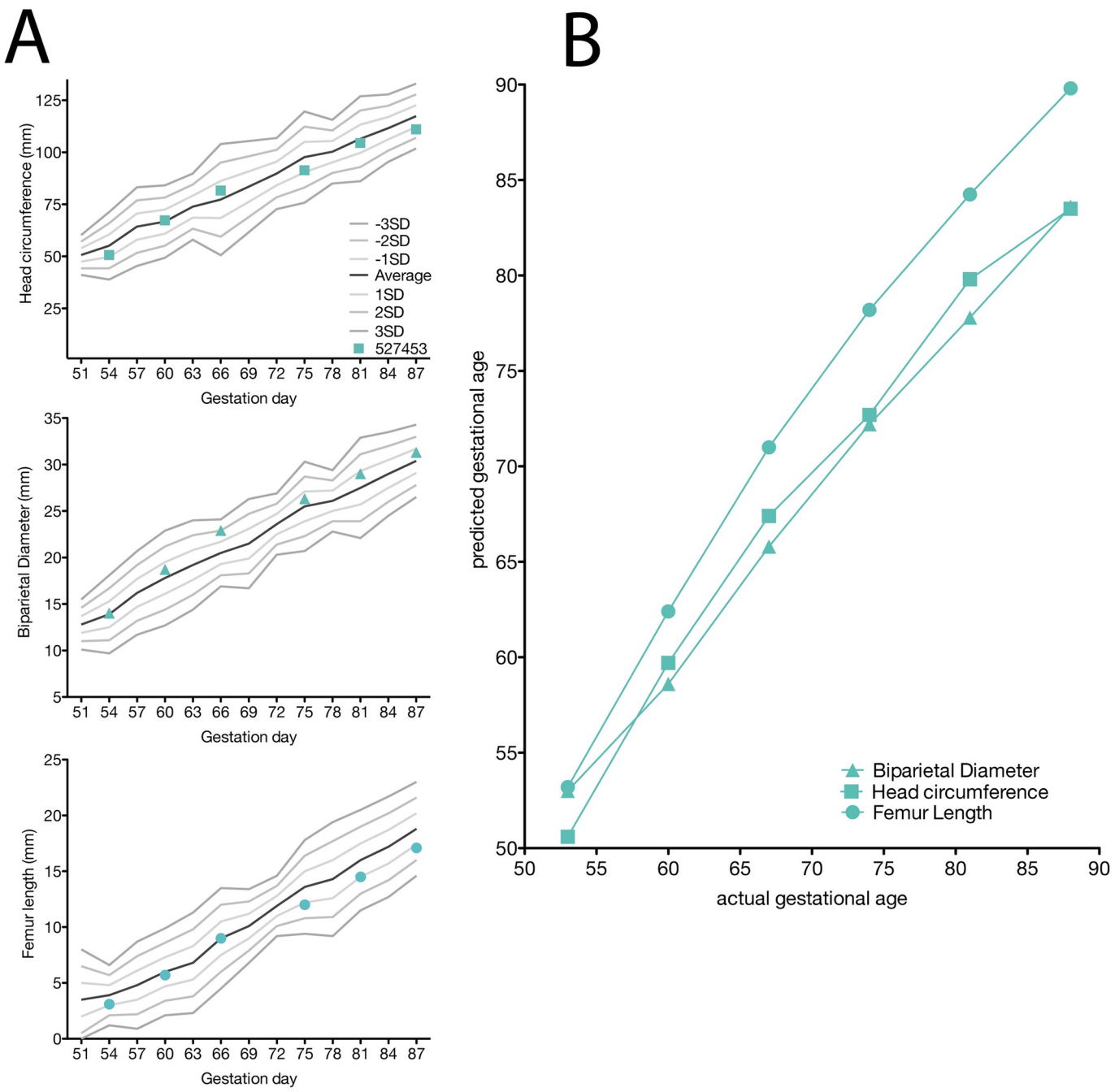

Fig 5. Fetal growth measured by ultrasonography. (A) Head circumference (HC), biparietal diameter (BPD), and femur length (FL) were measured in weekly ultrasounds. All measurements are depicted as millimeters (mm). The solid lines were derived from reference ranges from Tarantal et al. 2005 to show the mean (black lines) and one, two, and three standard deviations from the mean (grey lines). The HC, BPD, and FL were then plotted along these reference ranges to observe any deviations from the mean. (B) The pGA is plotted against the aGA (based on gestational age estimated from breeding and menstrual history). The pGA is shown separately for each measurement: BPD (triangle), HC (square), and FL (circle).

https://doi.org/10.1371/journal.pone.0190617.g005

Amniotic fluid collected during necropsy also contained vRNA (Fig 2) but did not contain replicating virus as assessed via plaque assay. The highest viral loads were detected in fetal colon and fetal lung tissue. Most organs of the fetal digestive system had detectable vRNA: stomach, jejunum, and colon. The presence of vRNA in fetal ocular structures, cerebrum, and

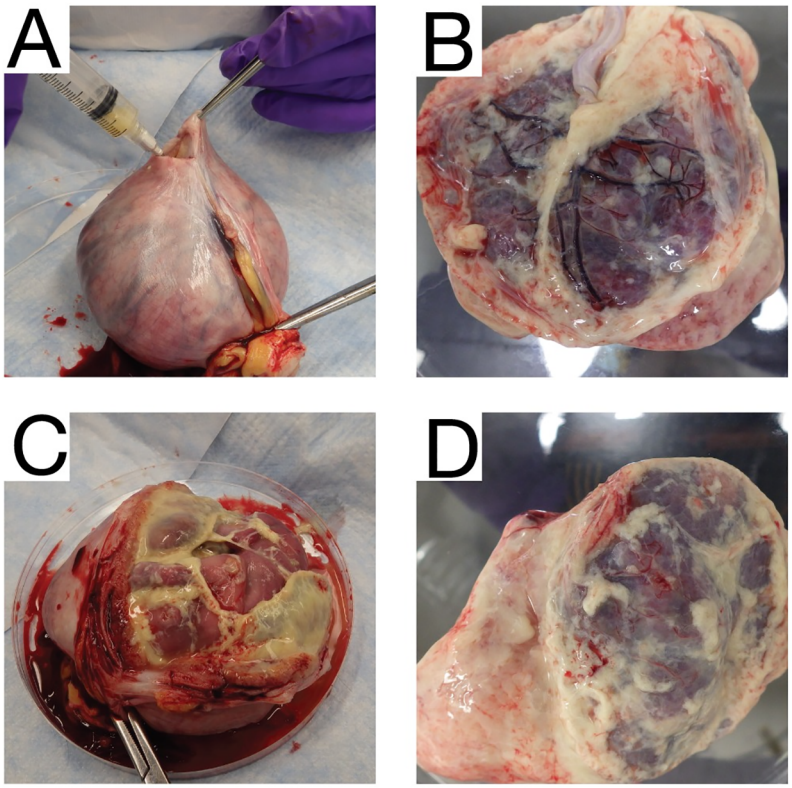

Fig 6. Maternal and fetal necropsy images. (A) The uterus was removed in entirety from the abdominal cavity of the dam using sterile instruments and a syringe was used to aspirate the purulent fluid from inside the uterine cavity. (B) The fetus was removed from the uterus and was covered in thick fibrinous material. Placental discs 1 (C) and 2 (D) were covered in the same thick fibrinous maternal that covered the fetus.

https://doi.org/10.1371/journal.pone.0190617.g006

dura mater indicates a central nervous system infection. vRNA was detected in four maternal lymph nodes and the spleen, indicating that ZIKV RNA was still present in the maternal immune system structures at 49 dpi, despite the absence of detectable maternal viremia.

Uteroplacental histopathology

Maternal-fetal interface tissues were evaluated for histological evidence of infection and lesions. There was clear evidence of both acute chorioamnionitis consistent with bacterial infection (Fig 7A), and features of relative placental insufficiency. There is no acute or chronic villitis, but the villi do show increased perivillous fibrin deposition (Fig 7B), and there are multiple remote infarctions (Fig 7C), which is a finding consistent with insufficiency. Radial arteries in the myometrium showed a pronounced leukocytoclastic vasculitis defined as an infiltrative mixture of lymphocytes, eosinophils, and plasma cells into the smooth muscle wall of these vessels (Fig 7D). The leukocytoclastic vasculitis seen around the radial arteries is usually related to hypersensitivity reactions or viral infections, and is not a consequence of bacterial infection [67]. The decidua basalis, placenta, placental bed and amniotic/chorionic membranes also showed significant pathology (S2 Table).

Fetal ocular histopathology

In our previous study [55], 2/2 macaque fetuses from first trimester ZIKV infection had suppurative inflammation in the ocular tissues at term (retina, choroid, optic nerve). In the

Table 1. Tissues with detectable ZIKV RNA from mother and fetus.

Tissue Source	Organ System	Tissue Name	vRNA copies/mg
Maternal	Immune	Axillary LN	258.3
		Inguinal LN	1774.8
		Mesenteric LN	9763.8
		Spleen	981.9
		Pelvic LN	583.7
	Reproductive	Decidua basalis	278.2
		Uterus	1471.7
		Uterus/placental bed	486.5
Fetal	Digestive System	Stomach	6140.4
		Colon	355157.0
		Jejunum	2055.9
		Liver	5.4
	Renal	Kidneys	51.1
		Urinary Bladder	185.1
	Cardiovascular	Aorta-thoracic	921.3
		Heart	366.0
		Pericardium	1196.3
	Extraembryonic	Amniotic Chorionic Membrane	4933.7
		Placental Disc 1	64.4
		Umbilical Cord	6.0
	Connective	Adipose Tissue-Omentum	5102.2
	Immune	Axillary LN	287.6
		Spleen	261.1
		Thymus	215.3
	Musculoskeletal	Muscle-quadriceps	387.0
	Pulmonary	Lung	37947.0
	Reproductive	Sem vesicle/Prostate	5700.0
		Testis	5188.1
	Central Nervous	Cerebrum 3 right*	72.9
		Dura Mater	74.3
	Ocular	Cornea	135.1
		Retina	316.5
		Sclera	370.8

127 maternal biopsies and fetal tissues were assayed for vRNA. All the tissues positive for ZIKV RNA are listed in this table. The maternal and fetal tissues which were vRNA negative are listed in S1 Table.

*Serial brain sections were performed, rather than specific dissection of brain structures, because of generalized autolysis.

https://doi.org/10.1371/journal.pone.0190617.t001

current study, ocular tissues were therefore carefully evaluated by qRT-PCR and histology. One fetal eye was dissected for vRNA detection by qRT-PCR and the contralateral eye was fixed and processed for histological analysis. ZIKV RNA was detected by qRT-PCR in the retina, choroid, and lens at low levels (Table 1). At the time of demise the fetal eyelids were still fused, suggesting that vRNA present in the eye was not due to passage of the virus from the amniotic fluid directly across the cornea or sclera.

In the fixed and processed globe, although grossly normal at necropsy, a chorioretinal coloboma affecting the ventral aspect of the globe was revealed with histological evaluation, and

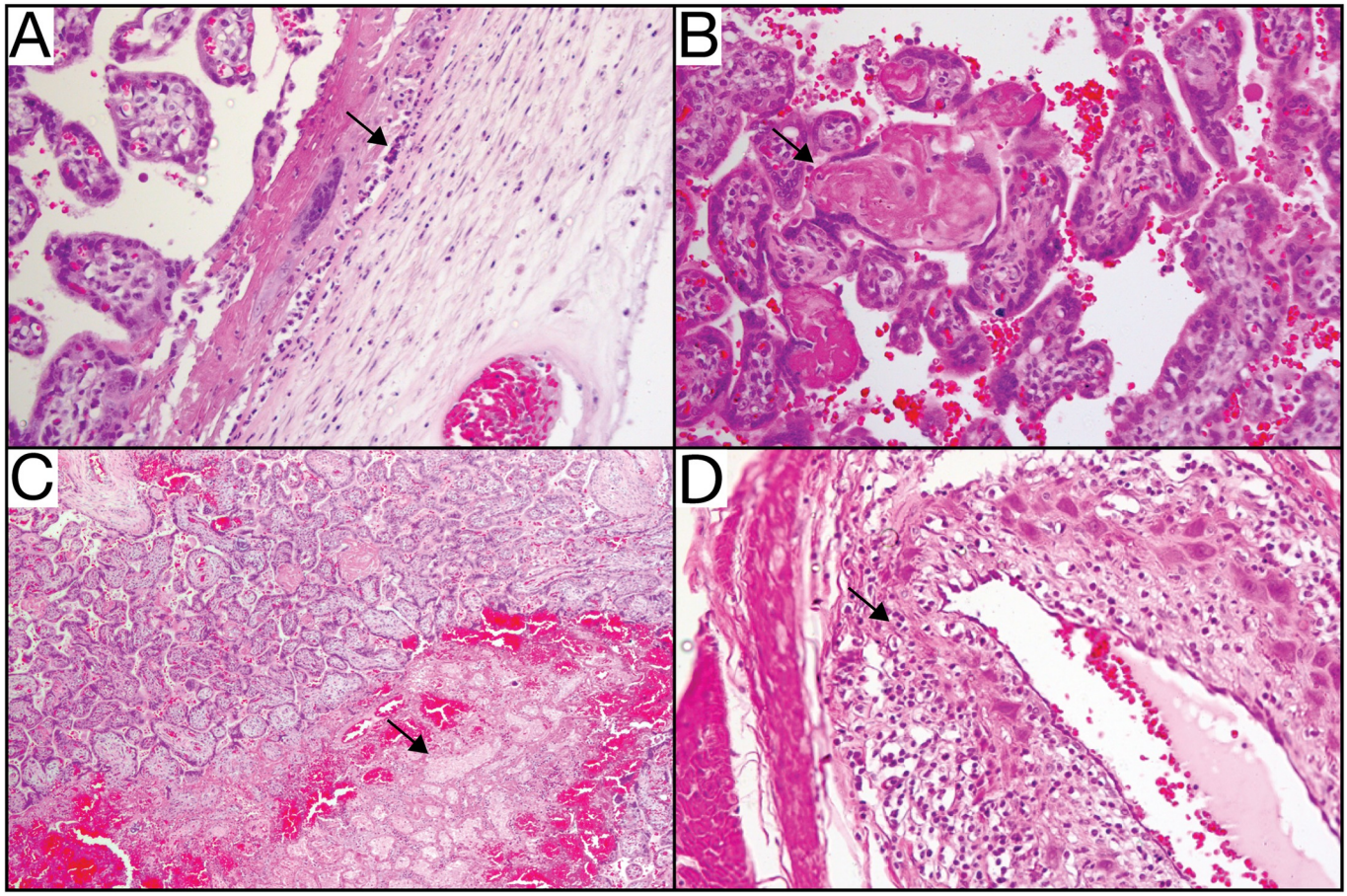

Fig 7. Uteroplacental histopathology from the primary placental disc. (A) Maternal neutrophils invading chorionic plate (arrow) is diagnostic of acute chorioamnionitis. (B) Villi show increased perivillous fibrin deposition (arrow) and there are multiple remote infarctions (arrow, C). (D) Radial arteries in the myometrium show a pronounced leukocytoclastic vasculitis (arrow) defined as an infiltrative mixture of lymphocytes, eosinophils, and plasma cells into the smooth muscle wall of these vessels.

https://doi.org/10.1371/journal.pone.0190617.g007

was characterized by extensive areas of choroidal and scleral thinning with a central area of choroidal and retinal pigmented epithelium absence and marked dysplasia of the adjacent retina (Fig 8). Additionally, the presence of fusion of the iris with the posterior corneal stroma and a seeming lack of adequate maturation of the iridocorneal angle structures suggested the presence of anterior segment dysgenesis. It is necessary to acknowledge that although the chorioretinal lesions were obvious even with a mild degree of autolysis, the histologic interpretation of the delicate structures of the developing anterior segment iridocorneal angle was hampered by the tissue autolysis present in the fetus. Although the chorioretinal lesions were obvious even with a mild degree of autolysis, making it impossible to definitively diagnose anterior segment dysgenesis. Because the retina is part of the central nervous system, the finding of retinal dysplasia indicates that the fetus had CNS abnormalities. However, no cerebral or cerebellar abnormalities were identified. The presence of the coloboma, dysplastic retina, and potential anterior segment dysgenesis are abnormalities that likely arose from disruption of early ocular developmental processes [68], consistent with the first trimester window of sensitivity in our earlier study [55].

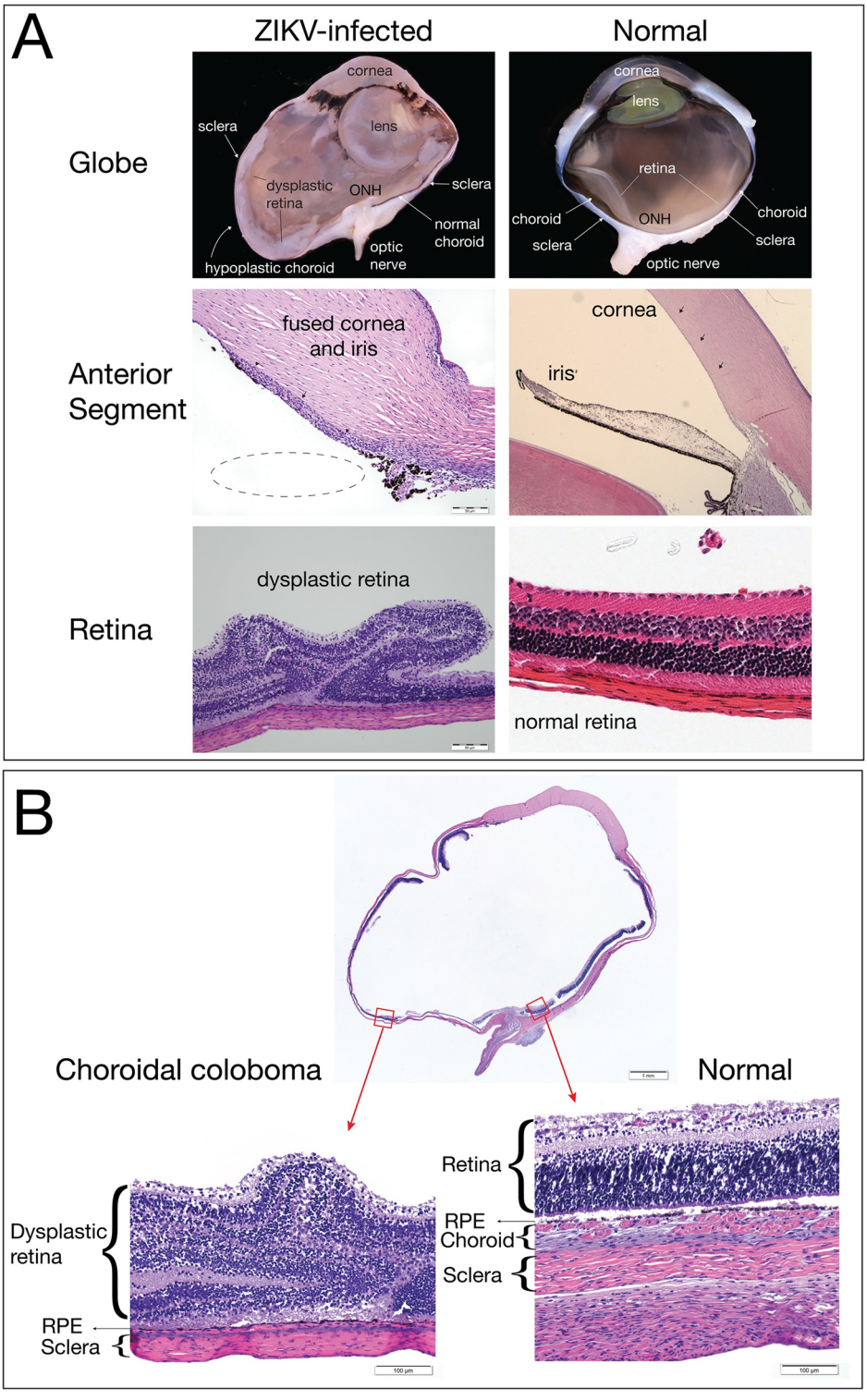

Fig 8. Fetal ocular pathology. (A) The left panels contain images of the ZIKV-infected eye, and the right panels show normal features from a control gestational day 155 male rhesus macaque fetus for comparison. The globe of the ZIKV-infected fetus shows a hypoplastic choroid and dysplastic retina compared to the normal eye. The irregular shape of the eye in the ZIKV-infected globe is a processing artifact. The anterior segment image of the ZIKV-infected fetus shows that the iris is fused to the posterior cornea (black arrow heads), suggesting anterior segment dysgenesis; the dotted line shows where the iris would be in normal ocular development. The ZIKV-infected eye presents marked retinal

dysplasia, characterized by retinal folding and loss of normal retinal organization when compared with the normal retina in the control image on the right. (B) A choroidal coloboma was identified on the ventral aspect of the globe (left image); the choroid had normal development on the dorsal aspect of the same globe (right image). The retina, retinal pigment epithelium (RPE), choroid (if present), and sclera are labeled with the left image demonstrating an absence of choroid.

https://doi.org/10.1371/journal.pone.0190617.g008

Maternal and fetal tissue pathology

Histologic lesions were noted in the fetal tissues that were potentially exposed to virus in the amniotic fluid, specifically the respiratory and gastrointestinal systems. There were significant lesions in the fetal lungs, fetal mesenteric lymph node, placenta, chorioamniotic membranes, decidua basalis, maternal uterus, and maternal spleen (S2 Table). We did not note any other pathological findings in the brain or the spinal cord. Consistent with the bacterial growth of *S. epidermidis* from amniotic fluid, gram positive cocci were observed within the lumen of the esophagus (S1 Fig), although there was no associated inflammatory reaction within the epithelium or deeper tissue layers of the esophagus. No other tissues had detectable bacteria as assessed by gram staining. The stomach and small intestine had mucosal autolysis with no discernible histologic lesions. The lumen of the colon had granular basophilic material consistent with nuclear debris.

The fetal lungs had notable pathology. The pulmonary alveoli had fibrin, cellular debris, edema, occasional squamous cells, and neutrophilic infiltration (alveolitis). There were multiple areas of alveoli with type II pneumocyte hyperplasia, with multifocal expansion of the alveolar septa with fibrin. The trachea, primary and secondary bronchi, however, had normal respiratory epithelium.

ZIKV histological analyses

ZIKV RNA localization was evaluated by ISH and mFISH on selected tissues with high vRNA burden as determined by qRT-PCR (Table 2). Fig 9 presents photomicrographs from near sections of the same spleen, fetal membranes, and fetal lung specimens. H&E staining is presented to demonstrate tissue organization and pathology; ISH to confirm the presence of ZIKV genome within cells, and mFISH for both negative and positive strand ZIKV RNAs to detect the dsRNA of replicative intermediates. S2 Fig also presents representative images of positive and negative strand RNAs for the tissues displayed; the merged figure colocalizes both positive and negative sense RNA strands, indicating active ZIKV replication in these tissues. Because of the degree of autolysis in the fetal brain tissues, it was not possible to process the tissues for ISH or mFISH.

Discussion

In this report of an adverse pregnancy outcome following ZIKV infection in a rhesus macaque, we describe fetal demise following suspected PPROM, fetal and maternal ZIKV burden, and significant ocular pathology in the fetus. ZIKV RNA was widely distributed throughout fetal tissues at necropsy, including in the cerebrum and ocular tissues. ZIKV vRNA was also identified in maternal lymph nodes and maternal spleen at the time of necropsy (49 dpi). Replication competent virus was identified by ISH for the presence of negative and positive strand RNA in fetal and maternal tissues. Although no brain pathology was noted, abnormal histology was observed in multiple fetal tissues including alveolitis and pneumocyte hyperplasia in fetal lung tissue, and severe ocular abnormalities. Both fetal ocular pathology and fetal demise have been described in human reports of ZIKV infection and demonstrate parallels between human and NHP CZS.

Table 2. Tissue vRNA burden, ISH and mFISH results.

Tissue Source	Tissue Name	vRNA copies/mg	ISH	mFISH
Maternal	Mesenteric LN	9763.8	-	
	Spleen	981.9	+	+
	Uterus	1471.7	+	+
	Decidua	278.2	+	+
Fetal	Amniotic/Chorionic Membrane	4933.7	+	+
	Colon	355157.0	+	+
	Stomach	6140.4	-	
	Pericardium	1196.3	-	
	Adipose Tissue-Omentum	5102.2	+	-
	Lung	37947.0	+	+
	Seminal Vesicle/Prostate	5700.0	-	
	Testis	5188.1	-	
	Eye (Retina/Cornea/Sclera)	316.5/135.1/370.8	-	

Tissues with a detectable vRNA burden were evaluated by ISH and mFISH. ISH detects positive sense vRNA; mFISH detects ZIKV replicative intermediates (negative and positive sense vRNA).

"+" indicates detectable signal in these tissues sections,

"-"indicates no signal. Tissues with no detectable ISH signal were not further evaluated by mFISH.

https://doi.org/10.1371/journal.pone.0190617.t002

Fetal demise

This is the first report of rupture of membranes and fetal demise in an NHP model of congenital ZIKV infection. We presume that maternal membranes ruptured by 42 dpi because we detected amniotic fluid markers in the urine at this time point, and identified high vRNA burden in this urine sample, despite absence of detectable maternal viremia at this time. It is possible that ZIKV RNA in the urine may represent vaginal secretions and not amniotic fluid leakage. ZIKV RNA has been detected in vaginal secretions collected by swab sampling up to 14 days after infection in humans [69] and nonhuman primates [54]. However, the likelihood of detecting ZIKV RNA in a pan urine collection from vaginal secretions would be highly unlikely and it is not clear what would have triggered a sudden onset of ZIKV RNA presence in vaginal secretions. In addition, maternal kidney, cervix and vagina did not have detectable vRNA at necropsy. A more likely scenario is one where the presence of ZIKV RNA in the urine represents ZIKV RNA in the amniotic fluid, as supported by a subsequent pregnancy loss associated with ZIKV RNA in fetal membranes and amniotic fluid. Collectively, these observations support the likelihood of the amniotic fluid as the source of vRNA in the pan urine collection.

A week after detection of ZIKV RNA in the pan-collected urine/amniotic fluid mixture, abdominal ultrasound evaluation found no fetal heartbeat and the fetus and dam were submitted for necropsy. There was no chronic villitis, which would be expected for viral induced changes. However, sections of the decidua and myometrium revealed a pronounced leukocytoclastic vasculitis involving the smooth muscle walls of the radial and spiral arteries. This is significant because this type of vasculitis is not expected in cases of bacterial infection, but does occur as a response to viral infections associated with cutaneous vasculitis (hypersensitivity vasculitis) [67]. Cutaneous vasculitis has not specifically been described in ZIKV infection, but vasculitis in the CNS has been described as the etiology of cerebral infarcts [70]. Although some placental lesions can be sporadically observed in unmanipulated pregnancies [71], the occurrence of decidual lesions in the case in this report, in parallel to the large placental infarct

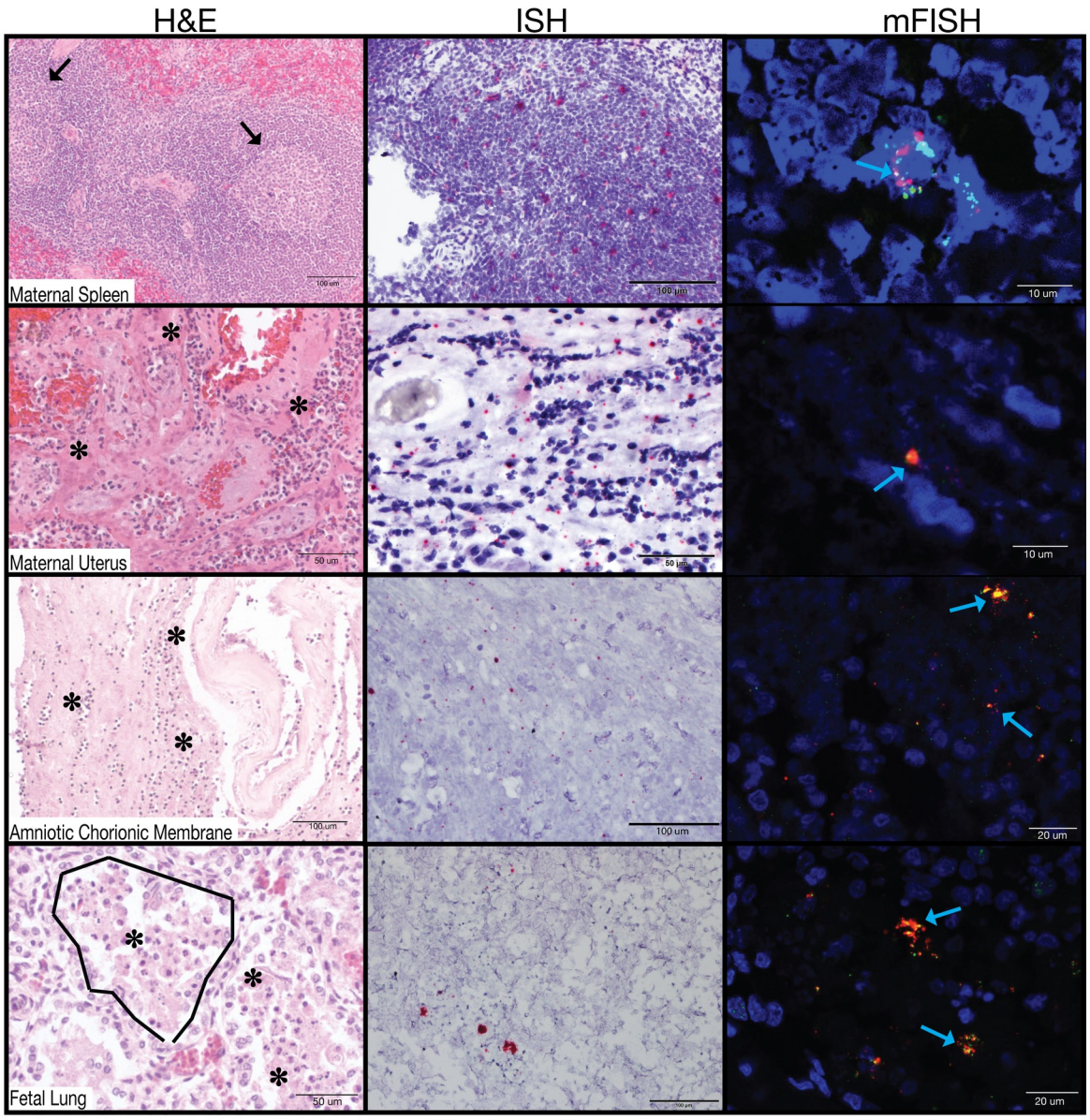

Fig 9. Tissue histology and viral localization of maternal spleen, maternal uterus, amniotic/chorionic membrane, and fetal lung. Each tissue was stained with H&E, ISH, and mFISH. ISH shows localization of ZIKV vRNA. mFISH shows replicative intermediates by staining the negative sense RNA strands green and positive sense RNA strands red. Co-localization (yellow) demonstrates dsRNA intermediates. Black arrows denote a germinal center. Asterisks indicate neutrophils. Blue arrows highlight green, red, or yellow fluorescence.

https://doi.org/10.1371/journal.pone.0190617.g009

which is unusual for this stage in gestation, suggests a role for ZIKV infection in this pathology.

Although there was fibrinopurulent material surrounding the fetus in the uterine cavity and gram positive cocci in the esophagus, multiple sections of placenta and all other fetal tissues had no histologic evidence of bacterial colonization. The growth of *S. epidermidis* from amniotic fluid was minimal. This was a surprise because we expected to find histologic evidence of bacteria throughout the placenta and parts of the fetus that were exposed to amniotic

fluid. Therefore, we considered the possibility of *S. epidermidis* environmental contamination in the amniotic fluid culture. Indeed, neutrophilic inflammation in the chorionic plate that is sterile has been described in human cases of PROM [72]. Sterile neutrophilic inflammation has also been reported previously in experimental infection in animal models with this ZIKV isolate, including mice which demonstrated neutrophil infiltration of the skeletal muscle and hippocampus [73] and male rhesus macaques which demonstrated interstitial neutrophilic prostatitis [51]. Therefore, while neutrophilic infiltration noted in our case is consistent with a bacterial intraamniotic infection, further studies will be able to provide clarification of the histopathologic outcomes at the maternal-fetal interface with ZIKV infection in macaque pregnancies.

Closely associated with this fetal demise is the occurrence of PPROM. Although it is not possible to determine if the amniotic membranes ruptured because of ZIKV infection or bacterial placentitis, the finding of PPROM followed by fetal demise also occurs during human prenatal ZIKV infection [24]. It could be hypothesized that the amniocentesis at 28 dpi contributed to the possible intrauterine bacterial infection; however, the long duration of time (21 days) separating these events, and the typical rapidity of preterm labor in the rhesus macaque with experimental bacterial infection of the amniotic fluid makes this unlikely [74, 75]. It is possible that the use of tylosin, a systemically absorbed bacteriostatic macrolide [76] commonly used for chronic diarrhea suppression in captive nonhuman primate colonies [77], contributed to bacterial growth suppression in a bacterial placentitis and masked signs of acute chorioamnionitis following the amniocentesis; this theory cannot be proved or disproved in this case report. Additional studies of ZIKV infection during NHP pregnancy are needed to determine if there is an association between congenital ZIKV infection and an increased risk for intraamniotic infection leading to PPROM and fetal demise. One may speculate that ZIKV infection early in gestation affects pregnancy-induced T-cell changes or placental invasion involved in uterine vascular remodeling necessary for normal blood flow to the placenta. In turn, ZIKV infection may lead to abnormal remodeling and abnormal blood flow to the placenta culminating in pathologic infarctions and increased risk for relative placental insufficiency and preterm birth, late pregnancy fetal demise, and stillbirth. This working hypothesis requires further study.

Fetal ocular defects

Congenital ocular abnormalities are strongly associated with human prenatal ZIKV infection, as demonstrated by the high frequency (up to 55%) of ocular disease in human infants with first trimester prenatal infections [12]. There is growing evidence that structures of the fetal visual system are a significant target for ZIKV in human pregnancy. The fetal eye evaluated for pathology in the current study had suspected anterior segment dysgenesis, a ventral choroidal coloboma, and retinal dysplasia. This is the first time that such severe ocular abnormalities have been reported with macaque CZS, and indeed, this birth defect has not been previously seen in the WNPRC colony. Bacterial infections are not associated with such abnormalities during development. In addition, an acute intrauterine bacterial infection would not have impacted eye development, since the ocular structure damage described would likely have occurred from the disruption of normal developmental processes which occur earlier in pregnancy. Anterior segment dysgenesis refers to a spectrum of developmental anomalies resulting from abnormalities of neural crest migration and differentiation during fetal development [78]. In humans, anterior segment dysgenesis is present in rare syndromes [79], and although the rate of anterior segment dysgenesis and related syndromes is unknown in rhesus macaques, it would be unlikely to appear in pregnancy.

An ocular coloboma is a congenital lesion associated with a failure in the closure of the embryonic (ocular) fissure causing defects of one or more ocular structures (i.e., the eyelids, lens, cornea, iris, ciliary body, zonules, choroid, retina and optic nerve). The defect is essentially a bare sclera with the overlying retinal pigmented epithelium, retina or choroid missing [80]. It may be sporadic or inherited and, in some cases, is associated with systemic disorders [80]. Choroidal colobomas in humans can be also associated with the presence of retinal dysplasia [81, 82], which was noted in the current case. Although there are multiple genetic mutations associated with colobomatous defects in humans [80], there is only one case report of a macaque with a coloboma, and no genetic evaluations were pursued in that report [83]. We did not pursue a genetic evaluation because it seems unlikely that a rare genetic defect would occur in one of the fetuses with congenital ZIKV infection. The defects in the eye affected the posterior and ventral aspect of the globe, which is common, since the ocular fissure is embryologically located in the ventro-nasal quadrant of the eye. It also mainly affected the choroid, thereby classifying it as a choroidal coloboma. The identification of retinal lesions and not cerebral or cerebellar lesions in this NHP case is not unexpected. The correlation between retinal lesions and cerebral or cerebellar lesions in humans is not known because most human cases of retinopathy do not have brain histology available. Animal models have identified retinal lesions without cerebral or cerebellar lesions [84].

In our previous study, we identified optic nerve gliosis in the two-first trimester infections [55], but did not identify other significant ocular pathology. CZS represents a continuum of disease from mild to severe and the macaque model highlights this by capturing the wide disease spectrum. It is also important to note that the current study was conducted with a virus stock prepared from an isolate obtained from a person infected in Puerto Rico, whereas our previous study [55] was conducted with a virus stock prepared from a French Polynesian isolate. Our results may indicate that closely related viruses can cause different outcomes in pregnant macaques, however further studies will be needed to understand whether specific genetic determinants are related to these outcomes. Although ZIKV causes ocular disease in the adult murine model [85], no ocular anomalies to this extent have yet been observed in mouse models of congenital ZIKV infection. This also underscores the important role the rhesus macaque model plays in studying ZIKV effects on pregnancy outcomes.

Maternal and fetal tissue viral distribution

ZIKV RNA was detected throughout fetal tissues, affecting multiple organ systems (digestive, respiratory, reproductive, cardiovascular, immune, and nervous), and replication competent virus was identified in fetal lung tissue 49 dpi via negative and positive strand RNA ISH. Remarkably, ZIKV RNA was also detected in maternal lymph nodes at 49 dpi and replication competent virus was identified in the lymph node tested. The presence of vRNA does not imply that the virus is replicating or may be transmissible. However, the detection of negative strand RNA by ISH and its colocalization with positive strand vRNA is confirmation of replication competent virus, and the finding of infectious virus in fetal and maternal tissues 49 dpi could have important implications for transmission. The fact that replication competent ZIKV is still present in an adult lymphoid-associated tissue at 49 dpi is critical to understanding the risk involved with organ transplantation, although with the caveat that viral persistence may be longer in pregnancy. Viral persistence is not explained by a lack of maternal humoral immune response since the dam developed neutralizing antibodies at concentrations similar to our previous NHP studies of ZIKV infections [56, 60].

We do not know to what extent ZIKV infection of the fetus directly contributed to fetal demise, since this case is complicated by PPROM with acute chorioamnionitis. Extended

exposure of the fetus to ZIKV is most likely responsible for the ocular pathology observed, and there is no literature of which we are aware which suggests that bacterial infection results in ocular malformations. The substantial viral burden in the fetal membranes also supports the hypothesis that ZIKV contributed to PPROM. The detection of replicating ZIKV intermediates in membranes and fetal tissues at the time of fetal demise also suggests that active ZIKV infection was ongoing up until fetal demise.

In summary, we describe a case of congenital ZIKV infection with severe ocular and uteroplacental pathology complicated by bacterial infection and fetal demise following apparent PPROM. The fetal ocular pathology recapitulates defects seen in human CZS. This is the first report of an adverse pregnancy outcome and fetal pathology in an NHP infected with ZIKV strain PRVABC59. Additional NHP studies with sham-infected animals as appropriate controls will be needed going forward to better define the baseline incidence of adverse pregnancy outcomes. This case report highlights the range of outcomes present in the macaque model along with our earlier NHP pregnancy studies [55] and supports development of the macaque model for not only defining the risk ZIKV poses for pregnant women and their fetuses in the Americas, but also for defining the precise pathways by which ZIKV accesses the fetal compartment, and for testing strategies to intervene in vertical transmission.

Supporting information

S1 Fig. Histology and gram stain of fetal esophagus. A) H&E image of the fetal esophagus. B) Gram stain of a section of the fetal esophagus epithelial surface, where gram positive cocci were abundant.
(TIF)

S2 Fig. Multiplex fluorescent in situ hybridization of positive and negative strand vRNA in fetal lung.
(TIF)

S1 Table. Tissues evaluated by qRT-PCR that were negative.
(TIF)

S2 Table. Histology description of fetal and maternal tissues.
(TIF)

Acknowledgments

Opinions, interpretations, conclusions, and recommendations are those of the author and are not necessarily endorsed by the U.S. Army.

Author Contributions

Conceptualization: Emma L. Mohr, Christina M. Newman, Dawn M. Dudley, David H. O'Connor, Thaddeus G. Golos.

Data curation: Emma L. Mohr, Lindsey N. Block, Christina M. Newman, Laurel M. Stewart, Michelle Koenig, Matthew Semler, Meghan E. Breitbach, Leandro B. C. Teixeira, Xiankun Zeng, Andrea M. Weiler, Gabrielle L. Barry, Gregory J. Wiepz, Dawn M. Dudley, Heather A. Simmons, Andres Mejia, Sarah Kohn, Kathleen M. Antony, Matthew T. Aliota, David H. O'Connor.

Formal analysis: Emma L. Mohr, Lindsey N. Block, Christina M. Newman, Laurel M. Stewart, Michelle Koenig, Matthew Semler, Meghan E. Breitbach, Leandro B. C. Teixeira, Xiankun

Zeng, Andrea M. Weiler, Gabrielle L. Barry, Troy H. Thoong, Gregory J. Wiepz, Dawn M. Dudley, Heather A. Simmons, Andres Mejia, Terry K. Morgan, M. Shahriar Salamat, Kathleen M. Antony, Matthew T. Aliota, Mariel S. Mohns, Thomas C. Friedrich, David H. O'Connor, Thaddeus G. Golos.

Funding acquisition: Saverio Capuano, III, David H. O'Connor, Thaddeus G. Golos.

Investigation: Emma L. Mohr, Lindsey N. Block, Christina M. Newman, Laurel M. Stewart, Michelle Koenig, Matthew Semler, Meghan E. Breitbach, Leandro B. C. Teixeira, Xiankun Zeng, Andrea M. Weiler, Gabrielle L. Barry, Troy H. Thoong, Dawn M. Dudley, Heather A. Simmons, Andres Mejia, Sarah Kohn, Kathleen M. Antony, Matthew T. Aliota, Mariel S. Mohns, Jennifer M. Hayes, Nancy Schultz-Darken, Michele L. Schotzko, Eric Peterson.

Methodology: Emma L. Mohr, Lindsey N. Block, Christina M. Newman, Dawn M. Dudley, Matthew T. Aliota, Shelby L. O'Connor, David H. O'Connor, Thaddeus G. Golos.

Project administration: Emma L. Mohr, Christina M. Newman, Dawn M. Dudley, David H. O'Connor, Thaddeus G. Golos.

Resources: Saverio Capuano, III, David H. O'Connor, Thaddeus G. Golos.

Software: Michelle Koenig, David H. O'Connor.

Supervision: Emma L. Mohr, Christina M. Newman, Dawn M. Dudley, Saverio Capuano, III, Jorge E. Osorio, Shelby L. O'Connor, Thomas C. Friedrich, David H. O'Connor, Thaddeus G. Golos.

Validation: Lindsey N. Block, Christina M. Newman, Laurel M. Stewart, Michelle Koenig, Matthew Semler, Meghan E. Breitbach, Leandro B. C. Teixeira, Xiankun Zeng, Andrea M. Weiler, Gabrielle L. Barry, Gregory J. Wiepz, Dawn M. Dudley, Heather A. Simmons, Andres Mejia, Sarah Kohn, Kathleen M. Antony, Matthew T. Aliota, Mariel S. Mohns, Jennifer M. Hayes, Nancy Schultz-Darken, Shelby L. O'Connor, Thomas C. Friedrich, David H. O'Connor, Thaddeus G. Golos.

Visualization: Emma L. Mohr, Lindsey N. Block, Heather A. Simmons, Andres Mejia, Kathleen M. Antony.

Writing – original draft: Emma L. Mohr, Lindsey N. Block, Christina M. Newman, Dawn M. Dudley, Heather A. Simmons, Andres Mejia, Matthew T. Aliota, Thomas C. Friedrich, David H. O'Connor, Thaddeus G. Golos.

Writing – review & editing: Emma L. Mohr, Lindsey N. Block, Heather A. Simmons, Andres Mejia, Terry K. Morgan, Thaddeus G. Golos.

References

1. Schuler-Faccini L, Ribeiro EM, Feitosa IM, Horovitz DD, Cavalcanti DP, Pessoa A, et al. Possible Association Between Zika Virus Infection and Microcephaly—Brazil, 2015. MMWR Morbidity and mortality weekly report. 2016; 65(3):59–62. Epub 2016/01/29. https://doi.org/10.15585/mmwr.mm6503e2 PMID: 26820244.
2. Rasmussen SA, Jamieson DJ, Honein MA, Petersen LR. Zika Virus and Birth Defects—Reviewing the Evidence for Causality. The New England journal of medicine. 2016. Epub 2016/04/14. https://doi.org/10.1056/NEJMsr1604338 PMID: 27074377.
3. van der Linden V, Filho EL, Lins OG, van der Linden A, Aragao Mde F, Brainer-Lima AM, et al. Congenital Zika syndrome with arthrogryposis: retrospective case series study. BMJ (Clinical research ed). 2016; 354:i3899. Epub 2016/08/12. https://doi.org/10.1136/bmj.i3899 PMID: 27509902.
4. van der Linden V, Pessoa A, Dobyns W, Barkovich AJ, Junior HV, Filho EL, et al. Description of 13 Infants Born During October 2015-January 2016 With Congenital Zika Virus Infection Without

Microcephaly at Birth—Brazil. MMWR Morbidity and mortality weekly report. 2016; 65(47):1343–8. Epub 2016/12/03. https://doi.org/10.15585/mmwr.mm6547e2 PMID: 27906905.

5. Honein MA, Dawson AL, Petersen EE, Jones AM, Lee EH, Yazdy MM, et al. Birth Defects Among Fetuses and Infants of US Women With Evidence of Possible Zika Virus Infection During Pregnancy. JAMA: the journal of the American Medical Association. 2017; 317(1):59–68. Epub 2016/12/14. https://doi.org/10.1001/jama.2016.19006 PMID: 27960197.
6. Russo FB, Jungmann P, Beltrao-Braga PC. Zika infection and the development of neurological defects. Cellular microbiology. 2017. Epub 2017/04/04. https://doi.org/10.1111/cmi.12744 PMID: 28370966.
7. Chan JF, Choi GK, Yip CC, Cheng VC, Yuen KY. Zika fever and congenital Zika syndrome: An unexpected emerging arboviral disease. The Journal of infection. 2016; 72(5):507–24. Epub 2016/03/05. https://doi.org/10.1016/j.jinf.2016.02.011 PMID: 26940504.
8. Costa F, Sarno M, Khouri R, de Paula Freitas B, Siqueira I, Ribeiro GS, et al. Emergence of Congenital Zika Syndrome: Viewpoint From the Front Lines. Annals of internal medicine. 2016; 164(10):689–91. Epub 2016/02/26. https://doi.org/10.7326/M16-0332 PMID: 26914810.
9. Franca GV, Schuler-Faccini L, Oliveira WK, Henriques CM, Carmo EH, Pedi VD, et al. Congenital Zika virus syndrome in Brazil: a case series of the first 1501 livebirths with complete investigation. Lancet. 2016. Epub 2016/07/04. https://doi.org/10.1016/s0140-6736(16)30902-3 PMID: 27372398.
10. Moore CA, Staples JE, Dobyns WB, Pessoa A, Ventura CV, Fonseca EB, et al. Characterizing the Pattern of Anomalies in Congenital Zika Syndrome for Pediatric Clinicians. JAMA pediatrics. 2016. Epub 2016/11/05. https://doi.org/10.1001/jamapediatrics.2016.3982 PMID: 27812690.
11. Meyer U, Yee BK, Feldon J. The neurodevelopmental impact of prenatal infections at different times of pregnancy: the earlier the worse? The Neuroscientist: a review journal bringing neurobiology, neurology and psychiatry. 2007; 13(3):241–56. Epub 2007/05/24. https://doi.org/10.1177/1073858406296401 PMID: 17519367.
12. Ventura CV, Maia M, Travassos SB, Martins TT, Patriota F, Nunes ME, et al. Risk Factors Associated With the Ophthalmoscopic Findings Identified in Infants With Presumed Zika Virus Congenital Infection. JAMA ophthalmology. 2016; 134(8):912–8. Epub 2016/05/27. https://doi.org/10.1001/jamaophthalmol.2016.1784 PMID: 27228275.
13. Zin AA, Tsui I, Rossetto J, Vasconcelos Z, Adachi K, Valderramos S, et al. Screening Criteria for Ophthalmic Manifestations of Congenital Zika Virus Infection. JAMA pediatrics. 2017. Epub 2017/07/18. https://doi.org/10.1001/jamapediatrics.2017.1474 PMID: 28715527.
14. Agrawal R, Oo HH, Balne PK, Ng L, Tong L, Leo YS. Zika Virus and Eye. Ocular immunology and inflammation. 2017:1–6. Epub 2017/03/21. https://doi.org/10.1080/09273948.2017.1294184 PMID: 28318359.
15. Ventura CV, Maia M, Bravo-Filho V, Gois AL, Belfort R Jr. Zika virus in Brazil and macular atrophy in a child with microcephaly. Lancet. 2016; 387(10015):228. Epub 2016/01/18. https://doi.org/10.1016/s0140-6736(16)00006-4 PMID: 26775125.
16. Ventura CV, Fernandez MP, Gonzalez IA, Rivera-Hernandez DM, Lopez-Alberola R, Peinado M, et al. First Travel-Associated Congenital Zika Syndrome in the US: Ocular and Neurological Findings in the Absence of Microcephaly. Ophthalmic surgery, lasers & imaging retina. 2016; 47(10):952–5. https://doi.org/10.3928/23258160-20161004-09 PMID: 27759862.
17. Ventura CV, Ventura LO, Bravo-Filho V, Martins TT, Berrocal AM, Gois AL, et al. Optical Coherence Tomography of Retinal Lesions in Infants With Congenital Zika Syndrome. JAMA ophthalmology. 2016; 134(12):1420–7. Epub 2016/11/11. https://doi.org/10.1001/jamaophthalmol.2016.4283 PMID: 27832267.
18. Ventura CV, Maia M, Ventura BV, Linden VV, Araujo EB, Ramos RC, et al. Ophthalmological findings in infants with microcephaly and presumable intra-uterus Zika virus infection. Arquivos brasileiros de oftalmologia. 2016; 79(1):1–3. Epub 2016/02/04. https://doi.org/10.5935/0004-2749.20160002 PMID: 26840156.
19. Miranda HA 2nd, Costa MC, Frazao MA, Simao N, Franchischini S, Moshfeghi DM. Expanded Spectrum of Congenital Ocular Findings in Microcephaly with Presumed Zika Infection. Ophthalmology. 2016; 123(8):1788–94. Epub 2016/05/30. https://doi.org/10.1016/j.ophtha.2016.05.001 PMID: 27236271.
20. Wong CW, Ng SR, Cheung CM, Wong TY, Mathur R. ZIKA-RELATED MACULOPATHY. Retinal cases & brief reports. 2017. Epub 2017/02/22. https://doi.org/10.1097/icb.0000000000000552 PMID: 28221261.
21. Yepez JB, Murati FA, Pettito M, Penaranda CF, de Yepez J, Maestre G, et al. Ophthalmic Manifestations of Congenital Zika Syndrome in Colombia and Venezuela. JAMA ophthalmology. 2017; 135(5):440–5. Epub 2017/04/19. https://doi.org/10.1001/jamaophthalmol.2017.0561 PMID: 28418539.

22. Centers for Disease Control and Prevention. Pregnant Women with Any Laboratory Evidence of Possible Zika Virus Infection in the United States and Territories [updated March 2, 2017; cited 2017 March 10]. https://www.cdc.gov/zika/geo/pregwomen-uscases.html.

23. Sarno M, Sacramento GA, Khouri R, do Rosario MS, Costa F, Archanjo G, et al. Zika Virus Infection and Stillbirths: A Case of Hydrops Fetalis, Hydranencephaly and Fetal Demise. PLoS neglected tropical diseases. 2016; 10(2):e0004517. Epub 2016/02/26. https://doi.org/10.1371/journal.pntd.0004517 PMID: 26914330 mc4767410.

24. Schaub B, Monthieux A, Najihoullah F, Harte C, Cesaire R, Jolivet E, et al. Late miscarriage: another Zika concern? European journal of obstetrics, gynecology, and reproductive biology. 2016; 207:240–1. Epub 2016/11/14. https://doi.org/10.1016/j.ejogrb.2016.10.041 PMID: 27837933.

25. van der Eijk AA, van Genderen PJ, Verdijk RM, Reusken CB, Mogling R, van Kampen JJ, et al. Miscarriage Associated with Zika Virus Infection. The New England journal of medicine. 2016. Epub 2016/07/28. https://doi.org/10.1056/NEJMc1605898 PMID: 27463941.

26. Martines RB, Bhatnagar J, Keating MK, Silva-Flannery L, Muehlenbachs A, Gary J, et al. Notes from the Field: Evidence of Zika Virus Infection in Brain and Placental Tissues from Two Congenitally Infected Newborns and Two Fetal Losses—Brazil, 2015. MMWR Morbidity and mortality weekly report. 2016; 65(6):159–60. Epub 2016/02/20. https://doi.org/10.15585/mmwr.mm6506e1 PMID: 26890059.

27. Morgan TK. Role of the Placenta in Preterm Birth: A Review. American journal of perinatology. 2016; 33 (3):258–66. Epub 2016/01/06. https://doi.org/10.1055/s-0035-1570379 PMID: 26731184.

28. Kapogiannis BG, Chakhtoura N, Hazra R, Spong CY. Bridging Knowledge Gaps to Understand How Zika Virus Exposure and Infection Affect Child Development. JAMA pediatrics. 2017; 171(5):478–85. Epub 2017/02/28. https://doi.org/10.1001/jamapediatrics.2017.0002 PMID: 28241263.

29. Prevention; CfDCa. Outcomes of Pregnancies with Laboratory Evidence of Possible Zika Virus Infection in the United States and the US Territories 2017 [cited 2017 August 1]. https://www.cdc.gov/zika/reporting/pregnancy-outcomes.html.

30. Racicot K, Cardenas I, Wunsche V, Aldo P, Guller S, Means RE, et al. Viral infection of the pregnant cervix predisposes to ascending bacterial infection. Journal of immunology (Baltimore, Md: 1950). 2013; 191(2):934–41. Epub 2013/06/12. https://doi.org/10.4049/jimmunol.1300661 PMID: 23752614.

31. Carroll T, Lo M, Lanteri M, Dutra J, Zarbock K, Silveira P, et al. Zika virus preferentially replicates in the female reproductive tract after vaginal inoculation of rhesus macaques. PLoS pathogens. 2017; 13(7): e1006537. Epub 2017/07/27. https://doi.org/10.1371/journal.ppat.1006537 PMID: 28746373.

32. Paz-Bailey G, Rosenberg ES, Doyle K, Munoz-Jordan J, Santiago GA, Klein L, et al. Persistence of Zika Virus in Body Fluids—Preliminary Report. The New England journal of medicine. 2017. Epub 2017/02/15. https://doi.org/10.1056/NEJMoa1613108 PMID: 28195756.

33. Sotelo JR, Sotelo AB, Sotelo FJB, Doi AM, Pinho JRR, Oliveira RC, et al. Persistence of Zika Virus in Breast Milk after Infection in Late Stage of Pregnancy. Emerging infectious diseases. 2017; 23(5):856–7. Epub 2017/02/14. https://doi.org/10.3201/eid2305.161538 PMID: 28192072.

34. Oliveira Souto I, Alejo-Cancho I, Gascon Brustenga J, Peiro Mestres A, Munoz Gutierrez J, Martinez Yoldi MJ. Persistence of Zika virus in semen 93 days after the onset of symptoms. Enfermedades infecciosas y microbiologia clinica. 2016. Epub 2016/12/23. https://doi.org/10.1016/j.eimc.2016.10.009 PMID: 28007310.

35. Atkinson B, Thorburn F, Petridou C, Bailey D, Hewson R, Simpson AJ, et al. Presence and Persistence of Zika Virus RNA in Semen, United Kingdom, 2016. Emerging infectious diseases. 2017; 23(4):611–5. Epub 2016/12/21. https://doi.org/10.3201/eid2304.161692 PMID: 27997333.

36. Gaskell KM, Houlihan C, Nastouli E, Checkley AM. Persistent Zika Virus Detection in Semen in a Traveler Returning to the United Kingdom from Brazil, 2016. Emerging infectious diseases. 2017; 23 (1):137–9. Epub 2016/10/18. https://doi.org/10.3201/eid2301.161300 PMID: 27748650.

37. Turmel JM, Abgueguen P, Hubert B, Vandamme YM, Maquart M, Le Guillou-Guillemette H, et al. Late sexual transmission of Zika virus related to persistence in the semen. Lancet. 2016; 387(10037):2501. Epub 2016/06/12. https://doi.org/10.1016/S0140-6736(16)30775-9 PMID: 27287833.

38. Hirayama T, Mizuno Y, Takeshita N, Kotaki A, Tajima S, Omatsu T, et al. Detection of dengue virus genome in urine by real-time reverse transcriptase PCR: a laboratory diagnostic method useful after disappearance of the genome in serum. Journal of clinical microbiology. 2012; 50(6):2047–52. Epub 2012/03/24. https://doi.org/10.1128/JCM.06557-11 PMID: 22442323.

39. de Laval F, Matheus S, Labrousse T, Enfissi A, Rousset D, Briolant S. Kinetics of Zika Viral Load in Semen. The New England journal of medicine. 2017; 377(7):697–9. Epub 2017/08/17. https://doi.org/10.1056/NEJMc1612600 PMID: 28813216.

40. Barzon L, Pacenti M, Franchin E, Lavezzo E, Trevisan M, Sgarabotto D, et al. Infection dynamics in a traveller with persistent shedding of Zika virus RNA in semen for six months after returning from Haiti to Italy, January 2016. Euro surveillance: bulletin Europeen sur les maladies transmissibles = European

communicable disease bulletin. 2016; 21(32). Epub 2016/08/20. https://doi.org/10.2807/1560-7917.es.2016.21.32.30316 PMID: 27542178.

41. Bandeira AC, Campos GS, Rocha VF, Souza BS, Soares MB, Oliveira AA, et al. Prolonged shedding of Chikungunya virus in semen and urine: A new perspective for diagnosis and implications for transmission. IDCases. 2016; 6:100–3. Epub 2016/11/25. https://doi.org/10.1016/j.idcr.2016.10.007 PMID: 27882301.

42. Barzon L, Pacenti M, Berto A, Sinigaglia A, Franchin E, Lavezzo E, et al. Isolation of infectious Zika virus from saliva and prolonged viral RNA shedding in a traveller returning from the Dominican Republic to Italy, January 2016. Euro surveillance: bulletin Europeen sur les maladies transmissibles = European communicable disease bulletin. 2016; 21(10). Epub 2016/03/19. https://doi.org/10.2807/1560-7917.es.2016.21.10.30159 PMID: 26987769.

43. Van den Bossche D, Cnops L, Van Esbroeck M. Recovery of dengue virus from urine samples by real-time RT-PCR. European journal of clinical microbiology & infectious diseases: official publication of the European Society of Clinical Microbiology. 2015; 34(7):1361–7. Epub 2015/03/22. https://doi.org/10.1007/s10096-015-2359-0 PMID: 25794553.

44. Iannetta M, Lalle E, Musso M, Carletti F, Scorzolini L, D'Abramo A, et al. Persistent detection of dengue virus RNA in vaginal secretion of a woman returning from Sri Lanka to Italy, April 2017. Euro surveillance: bulletin Europeen sur les maladies transmissibles = European communicable disease bulletin. 2017; 22(34). Epub 2017/09/01. https://doi.org/10.2807/1560-7917.es.2017.22.34.30600 PMID: 28857045.

45. Dupont-Rouzeyrol M, Biron A, O'Connor O, Huguon E, Descloux E. Infectious Zika viral particles in breastmilk. Lancet. 2016. Epub 2016/03/06. https://doi.org/10.1016/s0140-6736(16)00624-3 PMID: 26944028.

46. Arragain L, Dupont-Rouzeyrol M, O'Connor O, Sigur N, Grangeon JP, Huguon E, et al. Vertical Transmission of Dengue Virus in the Peripartum Period and Viral Kinetics in Newborns and Breast Milk: New Data. Journal of the Pediatric Infectious Diseases Society. 2016. Epub 2016/10/21. https://doi.org/10.1093/jpids/piw058 PMID: 27760799.

47. Meaney-Delman D, Oduyebo T, Polen KN, White JL, Bingham AM, Slavinski SA, et al. Prolonged Detection of Zika Virus RNA in Pregnant Women. Obstetrics and gynecology. 2016. Epub 2016/08/02. https://doi.org/10.1097/aog.0000000000001625 PMID: 27479770.

48. Driggers RW, Ho CY, Korhonen EM, Kuivanen S, Jaaskelainen AJ, Smura T, et al. Zika Virus Infection with Prolonged Maternal Viremia and Fetal Brain Abnormalities. The New England journal of medicine. 2016. Epub 2016/03/31. https://doi.org/10.1056/NEJMoa1601824 PMID: 27028667.

49. Suy A, Sulleiro E, Rodo C, Vazquez E, Bocanegra C, Molina I, et al. Prolonged Zika Virus Viremia during Pregnancy. The New England journal of medicine. 2016; 375(26):2611–3. Epub 2016/12/14. https://doi.org/10.1056/NEJMc1607580 PMID: 27959695.

50. de Souza Pereira BB, Darrigo Junior LG, de Mello Costa TC, Felix AC, Simoes BP, Stracieri AB, et al. Prolonged viremia in dengue virus infection in hematopoietic stem cell transplant recipients and patients with hematological malignancies. Transplant infectious disease: an official journal of the Transplantation Society. 2017. Epub 2017/05/06. https://doi.org/10.1111/tid.12721 PMID: 28475281.

51. Hirsch AJ, Smith JL, Haese NN, Broeckel RM, Parkins CJ, Kreklywich C, et al. Zika Virus infection of rhesus macaques leads to viral persistence in multiple tissues. PLoS pathogens. 2017; 13(3): e1006219. Epub 2017/03/10. https://doi.org/10.1371/journal.ppat.1006219 PMID: 28278237.

52. Aid M, Abbink P, Larocca RA, Boyd M, Nityanandam R, Nanayakkara O, et al. Zika Virus Persistence in the Central Nervous System and Lymph Nodes of Rhesus Monkeys. Cell. 2017. Epub 2017/05/02. https://doi.org/10.1016/j.cell.2017.04.008 PMID: 28457610.

53. Aid M, Abbink P, Larocca RA, Boyd M, Nityanandam R, Nanayakkara O, et al. Zika Virus Persistence in the Central Nervous System and Lymph Nodes of Rhesus Monkeys. Cell. 2017; 169(4):610–20.e14. Epub 2017/05/02. https://doi.org/10.1016/j.cell.2017.04.008 PMID: 28457610.

54. Osuna CE, Lim SY, Deleage C, Griffin BD, Stein D, Schroeder LT, et al. Zika viral dynamics and shedding in rhesus and cynomolgus macaques. Nature medicine. 2016; 22(12):1448–55. Epub 2016/11/01. https://doi.org/10.1038/nm.4206 PMID: 27694931.

55. Nguyen SM, Antony KM, Dudley DM, Kohn S, Simmons HA, Wolfe B, et al. Highly efficient maternal-fetal Zika virus transmission in pregnant rhesus macaques. PLoS pathogens. 2017; 13(5):e1006378. Epub 2017/05/26. https://doi.org/10.1371/journal.ppat.1006378 PMID: 28542585.

56. Dudley DM, Aliota MT, Mohr EL, Weiler AM, Lehrer-Brey G, Weisgrau KL, et al. A rhesus macaque model of Asian-lineage Zika virus infection. Nature communications. 2016; 7:12204. Epub 2016/06/29. https://doi.org/10.1038/ncomms12204 PMID: 27352279.

57. Enders AC. Implantation in the macaque: expansion of the implantation site during the first week of implantation. Placenta. 2007; 28(8–9):794–802. Epub 2006/12/26. https://doi.org/10.1016/j.placenta.2006.11.001 PMID: 17188351.

58. Blankenship TN, Enders AC, King BF. Trophoblastic invasion and the development of uteroplacental arteries in the macaque: immunohistochemical localization of cytokeratins, desmin, type IV collagen, laminin, and fibronectin. Cell and tissue research. 1993; 272(2):227–36. Epub 1993/05/01. PMID: 7685655.

59. Bondarenko GI, Burleigh DW, Durning M, Breburda EE, Grendell RL, Golos TG. Passive immunization against the MHC class I molecule Mamu-AG disrupts rhesus placental development and endometrial responses. Journal of immunology (Baltimore, Md: 1950). 2007; 179(12):8042–50. Epub 2007/12/07. PMID: 18056344.

60. Aliota MT, Dudley DM, Newman CM, Mohr EL, Gellerup DD, Breitbach ME, et al. Heterologous Protection against Asian Zika Virus Challenge in Rhesus Macaques. PLoS neglected tropical diseases. 2016; 10(12):e0005168. Epub 2016/12/03. https://doi.org/10.1371/journal.pntd.0005168 PMID: 27911897.

61. Adams Waldorf KM, Stencel-Baerenwald JE, Kapur RP, Studholme C, Boldenow E, Vornhagen J, et al. Fetal brain lesions after subcutaneous inoculation of Zika virus in a pregnant nonhuman primate. Nature medicine. 2016. Epub 2016/09/13. https://doi.org/10.1038/nm.4193 PMID: 27618651.

62. Tarantal AF. Ultrasound Imaging in Rhesus (Macaca mulatta) and Long-tailed (Macaca fascicularis) Macaques: Reproductive and Research Applications. Ultrasound Imaging: Elsevier Ltd.; 2005.

63. Tarantal AF, Hendrickx AG. Characterization of prenatal growth and development in the crab-eating macaque (Macaca fascicularis) by ultrasound. The Anatomical record. 1988; 222(2):177–84. Epub 1988/10/01. https://doi.org/10.1002/ar.1092220210 PMID: 3063137.

64. Lindsey HS, Calisher CH, Mathews JH. Serum dilution neutralization test for California group virus identification and serology. Journal of clinical microbiology. 1976; 4(6):503–10. Epub 1976/12/01. PMID: 1002829.

65. Rutanen EM, Pekonen F, Karkkainen T. Measurement of insulin-like growth factor binding protein-1 in cervical/vaginal secretions: comparison with the ROM-check Membrane Immunoassay in the diagnosis of ruptured fetal membranes. Clinica chimica acta; international journal of clinical chemistry. 1993; 214 (1):73–81. Epub 1993/01/31. PMID: 7680971.

66. Doyle L, Young CL, Jang SS, Hillier SL. Normal vaginal aerobic and anaerobic bacterial flora of the rhesus macaque (Macaca mulatta). Journal of medical primatology. 1991; 20(8):409–13. Epub 1991/10/01. PMID: 1803013.

67. Carlson JA, Chen KR. Cutaneous vasculitis update: neutrophilic muscular vessel and eosinophilic, granulomatous, and lymphocytic vasculitis syndromes. The American Journal of dermatopathology. 2007; 29(1):32–43. Epub 2007/02/08. https://doi.org/10.1097/01.dad.0000245198.80847.ff PMID: 17284960.

68. Gribnau AA, Geijsberts LG. Morphogenesis of the brain in staged rhesus monkey embryos. Advances in anatomy, embryology, and cell biology. 1985; 91:1–69. Epub 1985/01/01. PMID: 3880980.

69. Murray KO, Gorchakov R, Carlson AR, Berry R, Lai L, Natrajan M, et al. Prolonged Detection of Zika Virus in Vaginal Secretions and Whole Blood. Emerging infectious diseases. 2017; 23(1):99–101. Epub 2016/10/18. https://doi.org/10.3201/eid2301.161394 PMID: 27748649.

70. Landais A, Cesaire A, Fernandez M, Breurec S, Herrmann C, Delion F, et al. ZIKA vasculitis: A new cause of stroke in children? Journal of the neurological sciences. 2017. Epub 2017/11/11. https://doi.org/10.1016/j.jns.2017.10.045 PMID: 29122294.

71. Bunton TE. Incidental lesions in nonhuman primate placentae. Veterinary pathology. 1986; 23(4):431–8. Epub 1986/07/01. https://doi.org/10.1177/030098588602300413 PMID: 3750737.

72. Romero R, Miranda J, Chaemsaithong P, Chaiworapongsa T, Kusanovic JP, Dong Z, et al. Sterile and microbial-associated intra-amniotic inflammation in preterm prelabor rupture of membranes. The journal of maternal-fetal & neonatal medicine: the official journal of the European Association of Perinatal Medicine, the Federation of Asia and Oceania Perinatal Societies, the International Society of Perinatal Obstet. 2015; 28(12):1394–409. Epub 2014/09/06. https://doi.org/10.3109/14767058.2014.958463 PMID: 25190175.

73. Aliota MT, Caine EA, Walker EC, Larkin KE, Camacho E, Osorio JE. Characterization of Lethal Zika Virus Infection in AG129 Mice. PLoS neglected tropical diseases. 2016; 10(4):e0004682. Epub 2016/04/20. https://doi.org/10.1371/journal.pntd.0004682 PMID: 27093158.

74. Novy MJ, Duffy L, Axthelm MK, Sadowsky DW, Witkin SS, Gravett MG, et al. Ureaplasma parvum or Mycoplasma hominis as sole pathogens cause chorioamnionitis, preterm delivery, and fetal pneumonia in rhesus macaques. Reproductive sciences (Thousand Oaks, Calif). 2009; 16(1):56–70. Epub 2009/01/06. https://doi.org/10.1177/1933719108325508 PMID: 19122105.

75. Adams Waldorf KM, Rubens CE, Gravett MG. Use of nonhuman primate models to investigate mechanisms of infection-associated preterm birth. BJOG: an international journal of obstetrics and gynaecology. 2011; 118(2):136–44. Epub 2010/11/03. https://doi.org/10.1111/j.1471-0528.2010.02728.x PMID: 21040390.

76. Ji LW, Dong LL, Ji H, Feng XW, Li D, Ding RL, et al. Comparative pharmacokinetics and bioavailability of tylosin tartrate and tylosin phosphate after a single oral and i.v. administration in chickens. Journal of veterinary pharmacology and therapeutics. 2014; 37(3):312–5. Epub 2013/12/12. https://doi.org/10.1111/jvp.12092 PMID: 24325541.

77. Blackwood RS, Tarara RP, Christe KL, Spinner A, Lerche NW. Effects of the macrolide drug tylosin on chronic diarrhea in rhesus macaques (Macaca mulatta). Comparative medicine. 2008; 58(1):81–7. Epub 2008/02/01. PMID: 19793461.

78. Churchill A, Booth A. Genetics of aniridia and anterior segment dysgenesis. The British journal of ophthalmology. 1996; 80(7):669–73. Epub 1996/07/01. PMID: 8795384.

79. Reis LM, Semina EV. Genetics of anterior segment dysgenesis disorders. Current opinion in ophthalmology. 2011; 22(5):314–24. Epub 2011/07/07. https://doi.org/10.1097/ICU.0b013e328349412b PMID: 21730847.

80. Gregory-Evans CY, Williams MJ, Halford S, Gregory-Evans K. Ocular coloboma: a reassessment in the age of molecular neuroscience. Journal of medical genetics. 2004; 41(12):881–91. Epub 2004/12/14. https://doi.org/10.1136/jmg.2004.025494 PMID: 15591273.

81. Onwochei BC, Simon JW, Bateman JB, Couture KC, Mir E. Ocular colobomata. Survey of ophthalmology. 2000; 45(3):175–94. Epub 2000/11/30. PMID: 11094243.

82. Yanoff MS, J. W. Ocular Pathology. 7th ed: Saunders Elsevier; 2015.

83. Lin CC, Tso MO, Vygantas CM. Coloboma of optic nerve associated with serous maculopathy. A clinicopathologic correlative study. Archives of ophthalmology (Chicago, Ill: 1960). 1984; 102(11):1651–4. Epub 1984/11/01. PMID: 6548623.

84. Cui L, Zou P, Chen E, Yao H, Zheng H, Wang Q, et al. Visual and Motor Deficits in Grown-up Mice with Congenital Zika Virus Infection. EBioMedicine. 2017; 20:193–201. Epub 2017/06/07. https://doi.org/10.1016/j.ebiom.2017.04.029 PMID: 28583742.

85. Miner JJ, Sene A, Richner JM, Smith AM, Santeford A, Ban N, et al. Zika Virus Infection in Mice Causes Panuveitis with Shedding of Virus in Tears. Cell reports. 2016; 16(12):3208–18. Epub 2016/09/11. https://doi.org/10.1016/j.celrep.2016.08.079 PMID: 27612415.